



Tectonics and cycle system of the Cretaceous Songliao Basin: An inverted active continental margin basin



Pu-Jun Wang^{a,*}, Frank Mattern^{b,*}, N. Alexei Didenko^c, De-Feng Zhu^d, Brad Singer^e, Xiao-Meng Sun^a

^a College of Earth Sciences and Key-Lab for Evolution of Past Life & Environment in NE Asia, Jilin University, Changchun 130061, China

^b Department of Earth Science, Sultan Qaboos University, Muscat, Oman

^c Yu.A. Kosygin Institute of Tectonics and Geophysics, Far Eastern Branch of Russian Academy of Sciences, Khabarovsk, Russia

^d Institute of Exploration and Development of Daqing Oilfield Company Ltd., Daqing 163712, China

^e Department of Geoscience, University of Wisconsin-Madison, 1215 W. Dayton St., Madison, WI 57706, USA

ARTICLE INFO

Article history:

Received 22 November 2015

Received in revised form 16 May 2016

Accepted 17 May 2016

Available online 18 May 2016

Keywords:

Cretaceous Songliao Basin

Tectonic evolution

Model for an inverted continental margin basin

Subsidence rates

Mongol-North China Plate

Siberian Plate

Pacific Plate

Syn-rift

Post-rift

Structural inversion stages

ABSTRACT

Recent ICDP drilling and deep basin volcanic exploration of 3000 m below the surface in the Songliao Basin (SB) have highlighted the 3-D delineation of the basin. The integrated new data led us to reevaluate the basin tectonics, for which the basin type, basin evolution and a number of geodynamic aspects have been controversial topics. We outline the position of a main lithospheric scale detachment fault beneath the SB, based on apparent crustal scale displacements, Moho breaks, the thinning of the Moho transition zone beneath the SB and the changing mantle thickness. This fault interpretation is consistent with simple shear as the rift mechanism.

Based on a comprehensive analysis of the tectonic setting, underlying crust, structural style, sequence stratigraphy, subsidence history and volcanism, we propose an active continental margin model for the SB which shows some similarities to aulacogens but also notable differences. Situated between two Late Mesozoic active continental margins, the northern/northwestern Mongol–Okhotsk and the eastern Sikhote–Alin orogenic belts, the Cretaceous basin evolved on a pre-Triassic structurally weak basement mosaic. Its development began with regional mega-rifting from 150 to 105 Ma, followed by significant sagging between 105 and 79.1 Ma and ended with regional uplift and basin inversion from 79.1 to 64 Ma.

Three regional angular unconformities separate the basin fill into three respective tectono-stratigraphic sequences. (1) The syn-rift stage is characterized by widespread fault-bounded grabens and volcanogenic successions, corresponding upward to the Huoshiling, Shahezi and Yingcheng Formations. (2) The post-rift stage includes the Dengloulou, Quantou, Qingshankou, Yaojia and Nenjiang Formations. It is a special feature that the subsidence rate is abnormally high (mean of 103 m/Ma), and that flood basalt erupted along an axial wrench fault zone, associated with several marine intervals from the mid-Turonian to early Campanian (K_2qn to K_2n), possibly (not certainly) indicating incipient sea floor spreading characterized by Moho breaks along the basin axis in the SB around 88 Ma. Stretching stopped abruptly at approximately 79.1 Ma and was followed by uplift and rapid erosion (-145 m/Ma). (3) Recorded by the Sifangtai and Mingshui Formations the structural inversion stage included a continuous depocenter migration to the northwest. The basin was shrinking to demise as a result of changing subduction parameters of the Pacific subduction zone.

In addition to the three tectonic basin cycles, a cyclic basin fill pattern exists with three volcanic basin fill intervals of Huoshiling, Yingcheng, and upper Qingshankou Formations that alternate with sedimentary basin fill intervals of Shahezi, Dengloulou–Quantou, and Yaojia–Nenjiang Formations.

When determining the subsidence rates, we observed not only anomalously fast subsidence but also found an intricate link between the subsidence rate and type of basin fill. After each volcanic interval, the subsidence rates increased in a cyclic fashion during the sedimentary intervals. Thus, there is a system of three different types of important, basin-wide geological cycles that controlled the evolution of the SB.

The subsidence rate was especially high (up to 199 m/Ma) after the last volcanic episode at 88 Ma. In addition to thermal subsidence and loading by the basin fill as causative processes, we also consider magmatic processes related to asthenospheric upwelling beneath the SB. They involve the roof collapse of shallow, depleted magma chambers, the igneous accretion of initially hot, dense, basic rocks, and lithospheric delamination beneath the SB. The difference in the subsidence rates during the volcanic and sedimentary intervals may in part also have been due to heating-related uplift during the volcanic intervals. The particularly high subsidence during the Late Cretaceous sedimentary cycles was partly increased by transtension.

* Corresponding authors.

E-mail addresses: WangPJ@jlu.edu.cn (P.-J. Wang), frank@sq.u.edu (F. Mattern).

We put forward a general model for active continental margin basins. They are generally similar to aulacogens but display the following differences. In active continental margin basins, rifting depends on the subduction parameters that may cause strong to mild extension in the giant marginal region. The geochemical composition of the volcanic rocks is more calc-alkaline in nature because they are suprasubduction-related. These basins will eventually enter a post-rift sag stage that involves thermal subsidence. However, the basin will still be near an active continental margin, and, thus, some dip- and/or strike-slip faulting may occur coevally, depending on the subduction parameters. Sag cycles in active continental margin basins will likely include volcanism. Basin inversion will affect active continental margin basins. Such basins strike parallel to the respective continental margin. Thus, basin inversion by subduction/collision may be more intense than in the case of aulacogens, which do not tend to strike parallel to the continental margin. Basin inversion may also precede a collision due to changing subduction parameters. Subsidence behavior may also differ because many aspects of subsidence may be at work. Subsidence curves in active continental margin basins may be fairly individual. The application of our model only requires settings with the presence of one Pacific margin type.

© 2016 The Authors. Published by Elsevier B.V. This is an open access article under the CC BY-NC-ND license (<http://creativecommons.org/licenses/by-nc-nd/4.0/>).

Contents

1. Introduction	83
2. Methodology	84
3. Geological background	85
3.1. Pre-Permian	87
3.2. Permian and Triassic	87
3.3. Jurassic and Cretaceous	88
3.4. Cenozoic	89
3.5. Underlying crust and mantle	91
4. Basin controlling fault systems	91
4.1. The NNE-SSW striking fault system	91
4.2. The NW-SE and N-S striking fault systems	91
4.3. Detachment fault system	92
5. Tectono-stratigraphy of the Songliao Basin (SB)	92
5.1. Volcanism and sedimentation	92
5.2. The syn-rift tectono-stratigraphy (Tithonian to mid-Albian)	93
5.3. The post-rift tectono-stratigraphy (mid-Albian to mid-Campanian)	93
5.4. The structural inversion tectono-stratigraphy (mid-Campanian to Danian)	94
5.5. Basin reconfiguration	95
6. Discussion	96
6.1. Alternating volcanic and sedimentary cycles and basin subsidence	96
6.2. Tectonic basin evolution: overview	97
6.3. Causes of formation of the SB	98
6.4. Comparison between the SB as an active continental margin basin with aulacogens	98
7. Conclusions	99
Acknowledgments	100
References	100

1. Introduction

The Songliao Basin (SB), situated on the Mongol-North China Plate, reputedly contains China's largest oil field, the Daqing Field, which is one of the very few super giant fields in the world that produces lacustrine oil (e.g., Yang, 1985; Li et al., 1995). During the Late Jurassic and Early Cretaceous, hundreds of rift basins developed in Northeast Asia (Ren et al., 2002), covering an area of more than 4 million km² from Lake Baikal to the Sikhote-Alin Region in E-W direction and from the Mongol-Okhotsk Fold Belt to the Xilamulun River-Yanji Suture Zone in N-S direction, as shown in Figs. 1 and 2. The SB is a unique case among them as it evolved into the largest rift basin and because it is the only one with a sizable Upper Cretaceous basin fill. These Upper Cretaceous deposits may reach a thickness of up to 6000 m (Figs. 3 and 4) and represent the most important oil and gas generating sequence in China (Feng et al., 2010).

These features have attracted considerable attention, especially since the early 1980's with the beginning of the Chinese policy termed "open door". The attention is mainly paid to the basin's resources, its intriguing evolution and geodynamics. Several basin models have been proposed, including the back-arc (Ma et al., 1989), intra-cratonic

"polyphase" (Cheng, 1982) and rift basin models (Feng et al., 2010; He et al., 2014), as well as an Andean-type basin and range system (Wang et al., 2007a). Although meritorious, most of these models do not match some of the recent observations related to the SB and its geological development. This indicates that the basin type is not well understood.

The plate tectonic setting of the SB is the northeastern corner of the Mongol-North China Plate, which suggests a marginal rather than a cratonic setting. The Jurassic to Early Cretaceous Mongol-Okhotsk Collisional Belt are in the north and northwest, where the Siberian Plate was sutured to the Mongol-North China Plate (Bazhenov et al., 1999; Cogné et al., 2005). In addition, there is the Pacific subduction zone beneath the Mongol-North China Plate in the east, which formed the Sikhote-Alin Orogenic Belt during the Late Mesozoic and Neogene (Soloviev et al., 2006; Kemkin, 2008).

Oceanward-aging oceanic crust of the Pacific Plate progresses from the Cenozoic to the Jurassic (Fig. 1), implying that the continental boundary was not a typical Andean-type margin (Ramos, 2010). New results regarding the basin architecture show that the structural style of the SB has a polyphase evolution, and rifting is an important process (P.J. Wang et al., 2015).

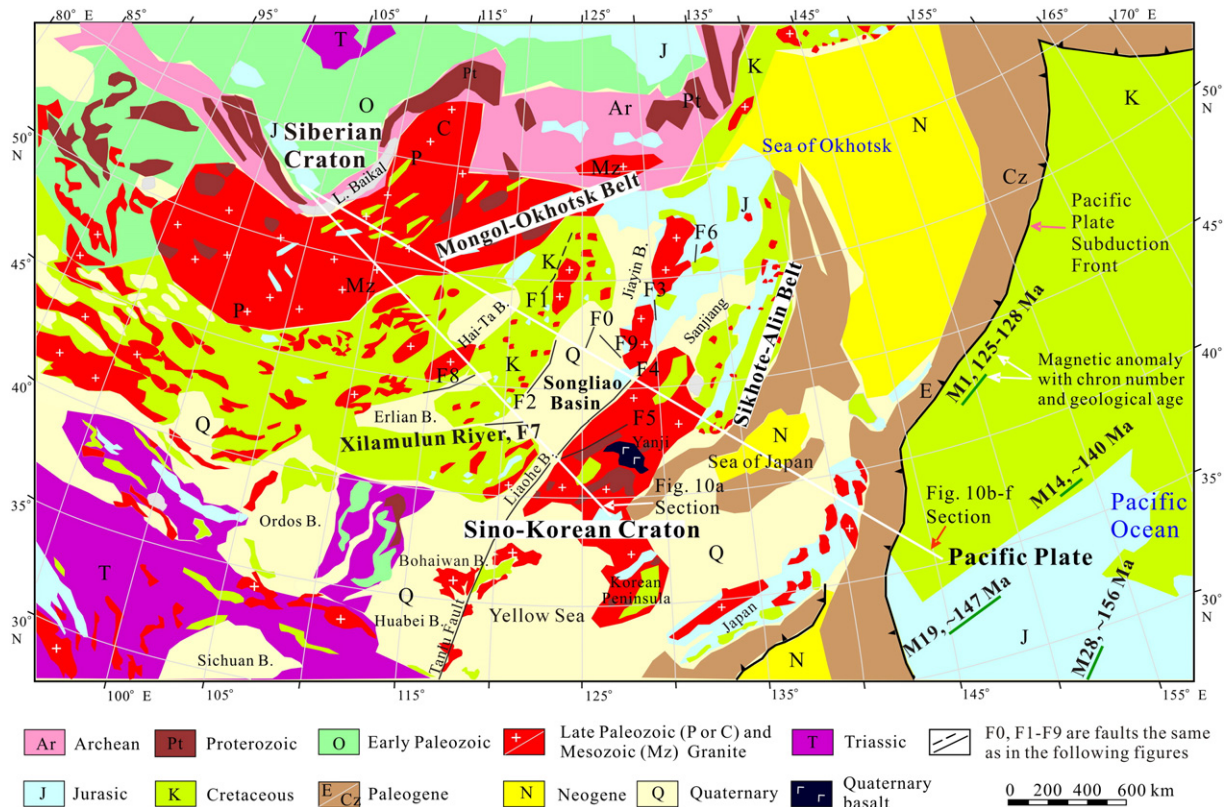


Fig. 1. Regional geological map of Northeast Asia with the SB located in the center, according to the International Geological Map of Asia (Ren et al., 2013). The two-sided active continental margin setting of the SB was characterized by the active orogenic belts of the northern/northwestern Mongol–Okhotsk and the eastern Sikhote–Alin belts during the Late Mesozoic. Note that the Pacific Ocean displays an aging seafloor, becoming older from the Cenozoic to the Jurassic with increasing distance from the continental margin, showing a “non-Andean” type of margin (cf. Ramos, 2010).

The precise life span and basin filling style of the SB are also key factors in reconstructing the basin’s evolution. Rapid progress has been made in recent years in understanding the SB and the regional geology, for example, through the China Cretaceous Continental Scientific Drilling in the SB (CCSD-SK) (Wang et al., 2013), which has been co-sponsored by the ICDP (International Continental Drilling Program) and the Chinese government. The drilling project coupled with petroleum exploration data have revealed detailed time sequences and 3-D filling patterns of the SB (e.g., Wang et al., 2009a; Wan et al., 2013). Accordingly, the recognition of both the chronostratigraphy and geochronology of the SB has significantly improved. For example, the syn-rift volcanogenic successions, previously believed to be “Jurassic” have been proven to be of Lower Cretaceous age (Jia et al., 2008; Wang et al., 2016). The project has thoroughly updated the temporal and spatial relationships among the SB’s stratigraphic and evolutionary history and the respective regional tectonic events. The new information provides us with an improved base to interpret the evolution of the SB.

Correlating the convergent history of the involved plates (Mongol–North China, Siberia and Pacific) with basin filling processes, we present a new successive fill model from the volcanic rift (150–105 Ma) via the sag stage coupled with a strike-slip component (105–79.1 Ma) to the tectonic inversion cycle (79.1–64 Ma). Whereas the first and last cycles are also found regionally and encompass the SB and its surroundings, the second cycle can only be found within the SB (Figs. 1 and 3).

We review some of the most recent advances that have been made in the characterization and understanding of the SB. We then intend to contribute to the understanding of the deep basin fault structure and continue by presenting new subsidence curves that help to explore the relationships among the alternating volcanic and sedimentary basin fill cycles on the one hand and changes in the subsidence rates on the other hand. In addition, we offer a fresh, new interpretative look at the SB, which we compare to aulacogens, making it easier to understand

and predict basin aspects. We consider the SB to be a two-sided active continental margin basin. Based on the differences that we note between aulacogens and the SB, we finally propose a new general model for “inverted active continental margin basins”.

2. Methodology

New data involved in this study include outcrop observations, borehole core sections, well loggings and 2-D/3-D seismic data that have been obtained from the ICDP drilling program since 2005 and from the deep basin exploration over the last 15 years which focused on the volcanic reservoirs below 3000 m (9843 ft) of buried depth (Wang and Chen, 2015). The outcrop sections were used for both facies analysis and the characterization of the paleobasin configuration. For example, recognition of outcrops of deep lake deposits at the present basin margin suggests that the present basin margin is an eroded margin for that particular sequence (Figs. 5d and 6d). In addition to the new data mentioned above, unpublished reports (e.g., Wang et al., 1991; Wang et al., 2007b) were used to draw facies maps (Fig. 6).

We utilized the deep borehole sections of SK-1n, SK-1s and SK-2 to create the basin fill sequences (Fig. 4) and the subsidence curves (Fig. 7). Conventional methods were employed for calculating the tectonic subsidence or subsidence due to conventional extension (i.e. normal faulting; compare Allen and Allen, 2005, p. 63–112, p. 266–327). To correct the primary sedimentary thickness, we followed the method described by Rieke and Chillingarian (1974, p. 87–122) for the compaction of the argillaceous sediments and that by Chillingarian and Wolf (1976, p. 69–114, p. 445–471) for the compaction of the siltstone, sandstone and conglomerate.

A comprehensive analysis was used for the most part in this study. To highlight the SB tectonics, we compiled data from different sources in the same figures to emphasize the basin filling and fault systems

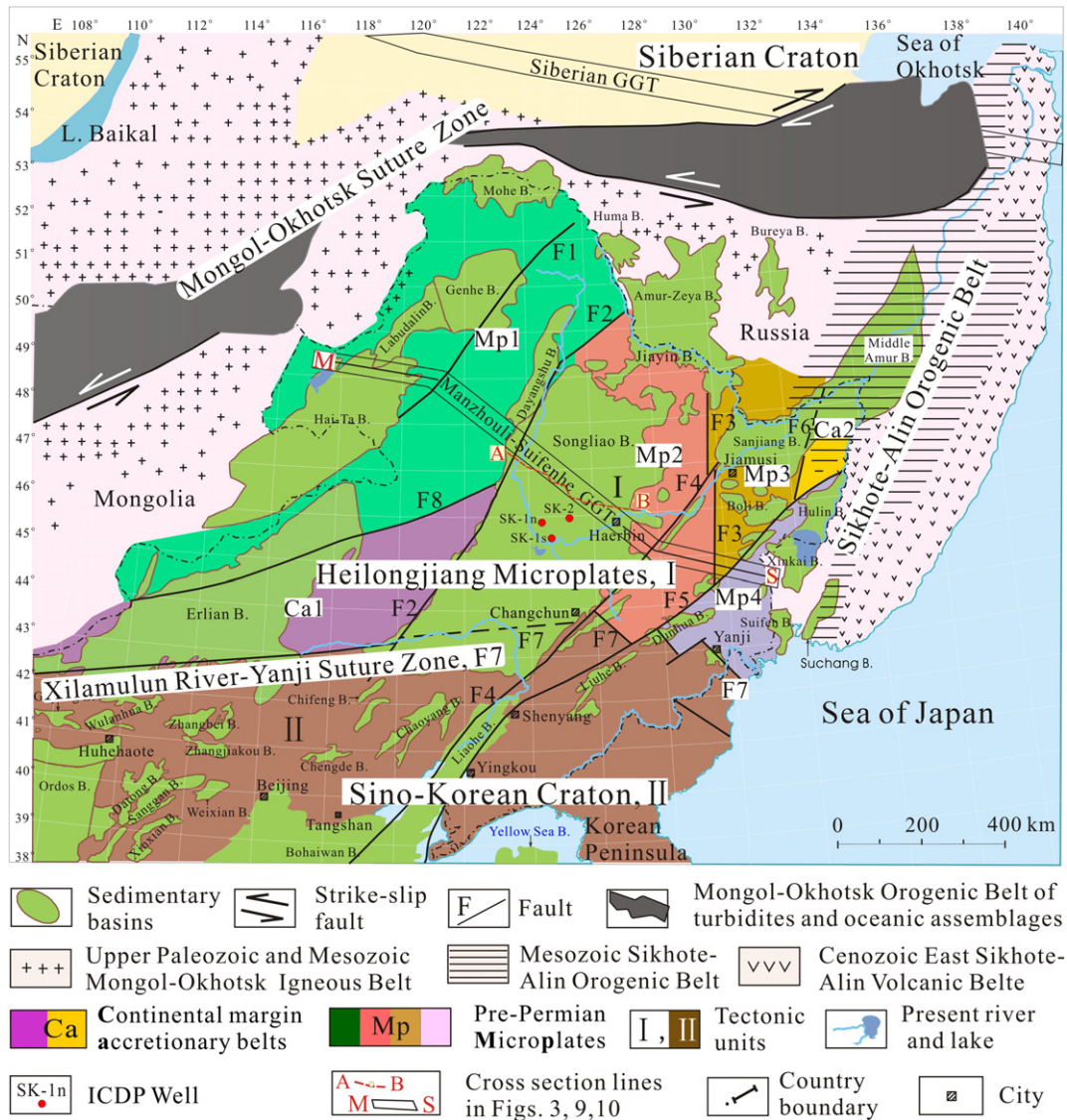


Fig. 2. Tectonic collage of the SB and its surroundings (adapted from Zhang et al. (1998); Karsakov and Zhao (2001); Li et al. (2012); Xu et al. (2014); Khanchuk et al. (2015); P.J. Wang et al. (2015)). The faults are: the Tayuan-Xijiatu Suture Zone (F1); Nenjiang-Balihan Fault (western boundary fault of the SB) (F2); Mudanjiang Suture Zone (F3); Jiamusi-Yitong Fault (eastern boundary fault of the SB) (F4); Dunhua-Mishan Fault (F5); Lower Heilongjiang or Dahezhen Fault (F6); Xilamulun River-Yanji Suture Zone (F7); and Heihe-Hegenshan Suture Zone (F8). The tectonic units are: the Mongol-Xing'an Microplate (Mp1); Songliao-Zhanguangcailing Microplate (Mp2); Jiamusi Massif of Archean age (Mp3); Khanka Massif of Early Palaeozoic (Mp4); Wenduermiao-Hegenshan Continental Margin Accretion Belt of Paleozoic age (Ca1); and Nadanhada Continental Margin Accretion Wedge of Jurassic age (Ca2). The assemblage of Mp2, Mp3, Mp4, and Ca1 are collectively termed "Heilongjiang Microplates" (I). Block-II indicates the Sino-Korean Craton. The so-called "Mongol-Jiamusi Block" (MJB) was constructed by the combination of Block-I and Mp1 before the Devonian (C.W. Wang et al., 2009). The Mongol-North China Plate was constructed when the Sino-Korean Craton and the MJB were welded together along the Xilamulun River-Yanji Suture Zone at the end of the Late Permian (Wang and Fan, 1997). By then, the pre-Triassic basement of the SB had been built up. GGT indicates Global Geosciences Transect.

(Fig. 3), the relationship between Moho structure and basalt eruption (Fig. 8) and the stratification of the underlying crust (Fig. 9). On the basis of a large amount of detailed geoscientific information concerning the depth structure, we propose the presence and position of a lithospheric scale detachment fault system beneath the SB (Fig. 9b).

3. Geological background

Concerning the regional geology and tectonics, the temporal and spatial relationships among the relative plates, orogenic belts and suture zones and tectono-stratigraphic sequences are most crucial to the evolution of the SB. The basement of the SB is a collage, pieced together from different microplates (Fig. 2). It was initially assembled during the Early Paleozoic (Zhang et al., 1998) and welded together with the Sino-Korean Craton by the Xilamulun River-Yanji Suture Zone at the end of

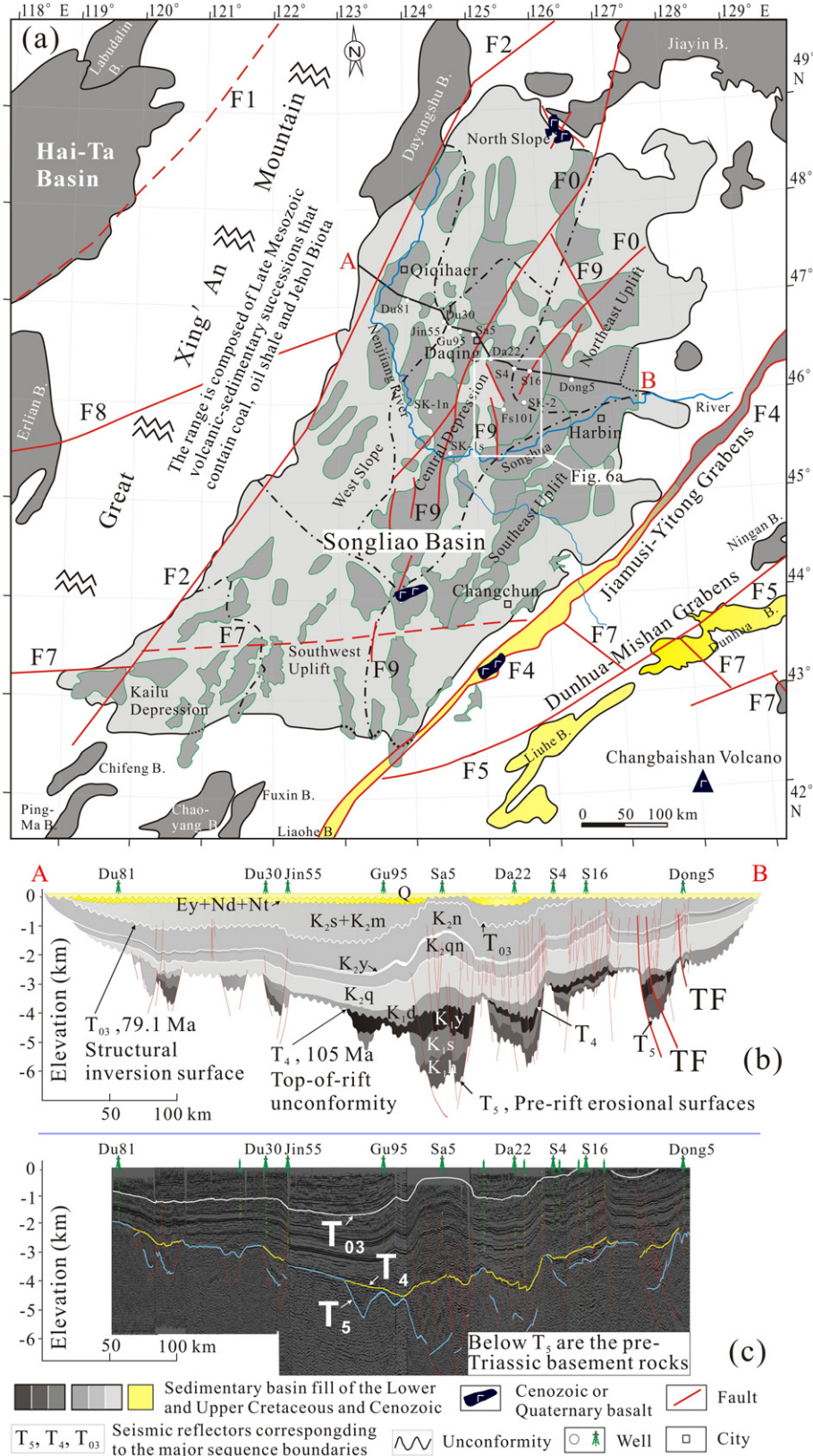
the Permian (Wang and Fan, 1997; Sun et al., 2005). During the Jurassic, the SB began its basin evolution on the pre-Triassic basement.

The basin fill of the syn-rift stage is composed of volcanogenic successions. Mega-rifting and volcanic eruptions occurred in the whole of Northeast Asia during this time (Figs. 1 to 3). Regional extension and general crustal thinning are revealed by graben structures, widespread volcanic rocks (Wang et al., 2006) and stretching of the underlying crust (Fig. 9).

During the syn-rift stage, two zones of plate convergence were active around the SB. To the north and northwest, the Mongol-Okhotsk Belt was in the late stage of being sutured to the Mongol-North China and Siberian plates (Cogné et al., 2005). The relative rotation among the blocks that was related to the suturing event lasted to the Late Cretaceous (Otofuji et al., 2006). The suturing and block rotation processes suggest an active margin setting during the Jurassic and Early Cretaceous for the Mongol-Okhotsk Belt. During the latter half of the

Mesozoic and the Neogene, the Mongol–Okhotsk Belt merged eastward with the Sikhote-Alin Belt, which originated from westward subduction of the Pacific Plate under the Eurasia (Soloviev et al., 2006; Kemkin, 2008). The active margin setting caused the reactivation of preexisting fault systems and the formation of new ones (Utkin, 2013). Considering

that the Mongol–North China Plate was created after the Xilamulun River–Yanji Suture Zone had formed during the Late Permian, the regional tectonics affecting the SB must have been mainly affected by the motions of the Siberian and/or Pacific plates at this evolutionary stage.



However, changes in the orientation of the boundary fault system suggest that the Siberian Plate may have played an important role during the giant regional extensional block faulting stage (150–105 Ma). As shown in Figs. 3a and 6a, the NW- and N-striking faults are the prevailing controlling boundary faults of the syn-rift grabens. In contrast, NNE or NE orientations of regional faults and basin axes became predominant after 105 Ma. Structural features with NNE or NE orientations are typically caused by tectonism in the Pacific Plate realm (Stepashko, 2006). Khanchuk et al. (2015) indicated that the suturing event of the Mongol–Okhotsk lasted to the Early Cretaceous and is characterized by a combination of magmatism and strike-slip movement along the suture zone (Fig. 2). It is, therefore, reasonable to infer that the orientation changes of the faults may indicate that the impact of the Pacific Plate on the SB evolution became dominant after 105 Ma. In other words, tectonic processes related to the history Mongol–Okhotsk suture zone may have contributed to the SB's tectonics significantly before 105 Ma.

In contrast to the regional syn-rift stage with volcanic graben structures, the post-rift stage is only developed in the SB. After the syn-rift stage, the SB continued to show a NNE basin orientation, and it displays a mainly epiclastic dish-shaped sag sequence (“dish-shaped” in cross section) that pinches out laterally (Figs. 3 and 4). The surface of the T₄ reflector in Figs. 3 and 4 is, therefore, considered to be the most important super-sequence boundary of the SB (Meng et al., 2005).

The structural inversion stage is characterized by regional compressional strains, recognized by the basin-wide folding of the previously deposited underlying sequences associated with uplift and erosion within and around the SB (Figs. 3b, 4c and 6e). Despite uplift and erosion, deposition continued. Uplift and erosion increased southeastward, and the basin depocenter shifted to the northwest, suggesting significant compressional stress from the southeast. The Mongol–North China and Siberian plates were welded together after the late Aptian (ca. 116 Ma; Cogné et al., 2005). Thus, the regional strain was caused by the interaction of the Eurasian and Pacific plates. The abrupt change from fast subsidence to uplift in the SB (at ca. 79.1 Ma, reflector T₀₃ in Figs. 3b and 4c) was likely due to the significant change of the Pacific Plate motion, both in direction and speed, during the Campanian (Maruyama and Seno, 1986; Stepashko, 2006; Didenko et al., 2014) (Fig. 10).

The collision of India with Asia and the opening of the Sea of Japan were momentous Cenozoic events for Asia's geology (Lee et al., 1999; White and Lister, 2012) that could have potentially impacted the SB. Three collisional intervals between the Indian and Eurasian Plates have been recorded; they can be subdivided into a soft collision between 60 and 44 Ma, an early hard collision from 44 to 22 Ma and a late hard collision from 22 Ma to the present (Kumar et al., 2007; Liu et al., 2009). The evolutionary history of the SB fill lasted from 150 Ma to 64 Ma. After the mid-Danian, the SB has neither experienced significant sedimentation nor significant deformation that can be recognized in geological cross sections, vertical sequences, facies associations and subsidence curves (Figs. 3b, 4, 6 and 7). Therefore, the collision had no significant influence on the SB's evolution, although the geological map of Asia (Ren et al., 2013) shows that the present landforms and geological features of Northeast Asia may have been profoundly impacted by the Indian Plate collision. For example, the Baikal Rift was created at the southeastern margin of the rigid Siberian Craton (Fig. 1) due to strike-slip motion, related to the indentation of the Indian Plate during the Cenozoic (e.g., Petit and Déverchère, 2006 and sources therein).

Thus, the stress induced by the Indian collision took effect in other parts of NE Asia but dissipated in the vicinity of the SB.

The Sea of Japan experienced Neogene rifting and subsequent contraction, caused by the collision of Japan with the Izu-Bonin Arc. Sedimentation and volcanism took place predominantly during the early to mid-Miocene (Yoon et al., 2014). The opening of the Sea of Japan belongs to a series of Cenozoic tectonic events, causing modifications of the original eastern Eurasian margin that were preponderantly characterized by divergence/extension and transform movement (e.g., Itoh et al., 2006 and sources therein). Because the SB had been well preserved since the mid-Danian (ca. 64 Ma) (see above), the opening of the Sea of Japan had no recognizable influence on the SB evolution either.

3.1. Pre-Permian

The center of Fig. 2 shows the area of the “Heilongjiang Microplates” (HMP). This is an association of microplates and a continental accretion zone (Mp2, Mp3, Mp4, Ca1 in Fig. 2) that was assembled during the early Paleozoic. The so-called “Mongol–Jiamusi Block (MJB)” was initially constructed during the Late Silurian by the combination of the HMP and the Mongol–Xin'an Block (Mp1 in Fig. 2), when the related suture zones F₁ and F₈ formed (C.W. Wang et al., 2009). The MJB constitutes the northern part of the present Mongol–North China Plate and is located between the Mongol–Okhotsk and Xilamulun River–Yanji suture zones (Fig. 2). The Mongol–Okhotsk Ocean opened during the Silurian within the Early Paleozoic collage (Bussien et al., 2011 and sources therein), and its oceanic lithosphere was continuously subducted during the Late Paleozoic (Kelty et al., 2008). The basement of the SB and adjacent areas are mainly composed of pre-Permian microplates (Mp1–Mp4) and continental margin accretionary belts (Ca1–Ca2) (Fig. 2). These microplates contain Proterozoic or Archean gneiss, granulite, schist and marble, Paleozoic sedimentary and volcanic rocks, slate, phyllite and schist (IGS, 1991). Bounding the microplates are suture zones (F7 and F8 in Fig. 2) and large fault systems (F2–F6 in Fig. 2) that cut down deeply to the Moho (Figs. 9 and 10). The suture zones include Paleozoic ophiolite suites, blueschists and deep marine deposits (Zhou et al., 2010a). They formed mainly during the Cambrian and Upper Mississippian (Zhang et al., 1998), although continued shortening may have lasted until the Early Mesozoic, especially in the eastern part of the MJB (Ca2 in Fig. 2) (Zhou et al., 2010b; Xu et al., 2013).

Each of the microplates may contain smaller blocks that are sutured by subordinate belts, such as the suture zone F1 in Fig. 2 (Zhou et al., 2010b). The continental margin accretionary belts (Ca1, Ca2 in Fig. 2) are composed of strongly deformed complex suites of sedimentary, volcanic and igneous rocks, slate, phyllite and schist (HGS, 1993). The western section (Ca1 in Fig. 1) formed during the Devonian (Zhang et al., 1998). The eastern counterpart (Ca2 in Fig. 1) formed during the Late Paleozoic to Mesozoic and gradually merged eastward with the Sikhote–Alin Fold Belt (Wu et al., 2011; Kemkin, 2008).

3.2. Permian and Triassic

The Paleo-Asian Ocean closed during the Permian (Li, 2006) creating the Xilamulun River–Yanji Suture Belt (F7 in Fig. 2), which united the Sino–Korean Craton in the south with the Mongol–Jiamusi Block (MJB) in the north (Sun et al., 2013). Thus, the Mongol–North China Plate was constructed (Wang and Fan, 1997; Sun et al., 2005). During most

Fig. 3. Basin fill of the SB: (a) Map view, showing Lower Cretaceous segmented volcanogenic grabens (dark gray) covered by the basin-wide post-rift sedimentary sequence of the Upper Cretaceous (light gray). (b) Cross-section of basin fill, interpreted with borehole-constrained seismic data. (c) Seismic reflection profile corresponding to Fig. b. Distribution of faults, basins, and basalt are adapted from JGS, 1988; HGS, 1993; Liu et al. (2001); Sun et al. (2006, 2010); Wang and Chen (2015). SK-1n, SK-1s, and SK-2 are boreholes from the ICDP drilling project. The central fault system is composed of NW–SE to N–S (F9) and NE–SW (F0) faults. The other faults are the same as in Fig. 2. The Lower Cretaceous grabens are stratigraphically bound between the seismic reflectors of T₅, the pre-rift erosional surface, and T₄, the top-of-rift unconformity. Formation symbols: K₁h is Huoshiling, K₁s is Shahezi, K₁y is Yingcheng, K₁d is Denglouku, K₂q is Quantou, K₂qn is Qingshankou, K₂y is Yaojia, K₂n is Nenjiang, K₂s is Sifangtai, K₂m is Mingshui. Note: (1) The major thrust-like faults (TF in b) of the eastern section cut all of the layers from the bottom to the top of the sequence; (2) the folds on the top of the K₂n formed from the eastern basin margin to the center of the SB; (3) the erosional truncation becomes more intense eastwards, as shown in b; and (4) the uplifted Upper Cretaceous sequences (K₂q and above) are widespread exposed in the eastern and southern parts of the SB (cf. Fig. 6c–e). All of these features imply a continuous compression since the end of K₂n (~79.1 Ma, mid-Campanian, cf. Fig. 4).

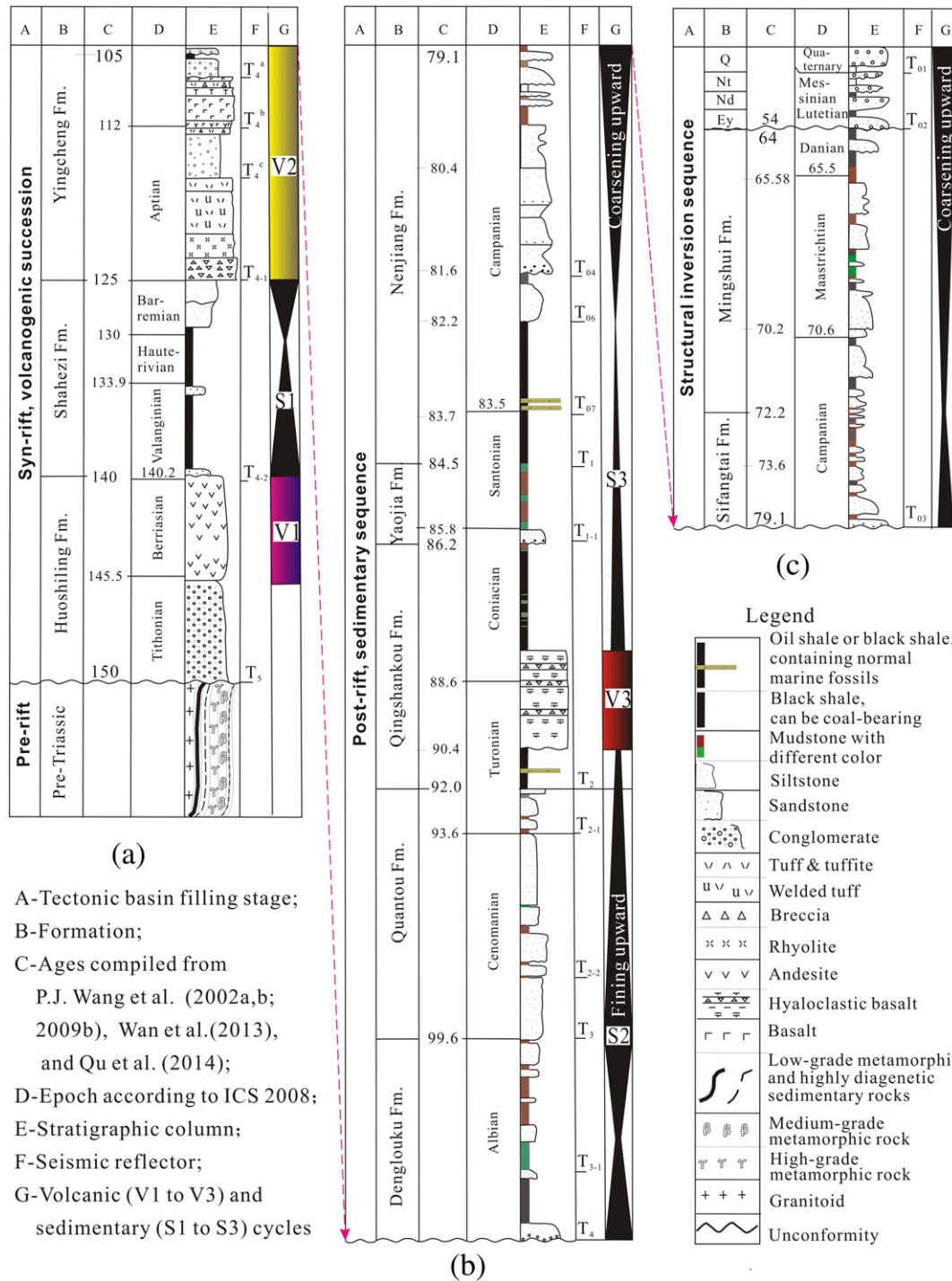


Fig. 4. Vertical basin fill sequence of the SB, showing: (1) three tectono-stratigraphic successions of syn-rift (a), post-rift (b) and structural inversion (c); (2) three episodes of volcanism at 145–140 Ma, 125–105 Ma, and close to 88 Ma, and; (3) several events of marine incursions from the mid-Turonian to lower Campanian.

of the Triassic period, the entire SB and the area to the west have experienced regional uplift and erosion because Triassic records are commonly absent (to the west of fault F4 in Fig. 2). To the east of the SB, Triassic deposits of marine and non-marine sediments and volcanic rocks locally accumulated (HGS, 1993). They generally display an angular unconformity with their overlying strata (JGS, 1988). Triassic rocks are more frequently found along the Xilamulun River-Yanji Suture Zone (F7 in Fig. 2). They mainly include kimberlite and syenite plutons,

suggesting a form of post-collisional decratonization of the northern margin of the Sino-Korean Craton (Peng et al., 2008; Yang et al., 2010).

3.3. Jurassic and Cretaceous

Three important geological events successively affected the SB during the Jurassic and Cretaceous. The first event was the formation of the Mongol–Okhotsk Suture Zone during the Jurassic (Zorin, 1999;

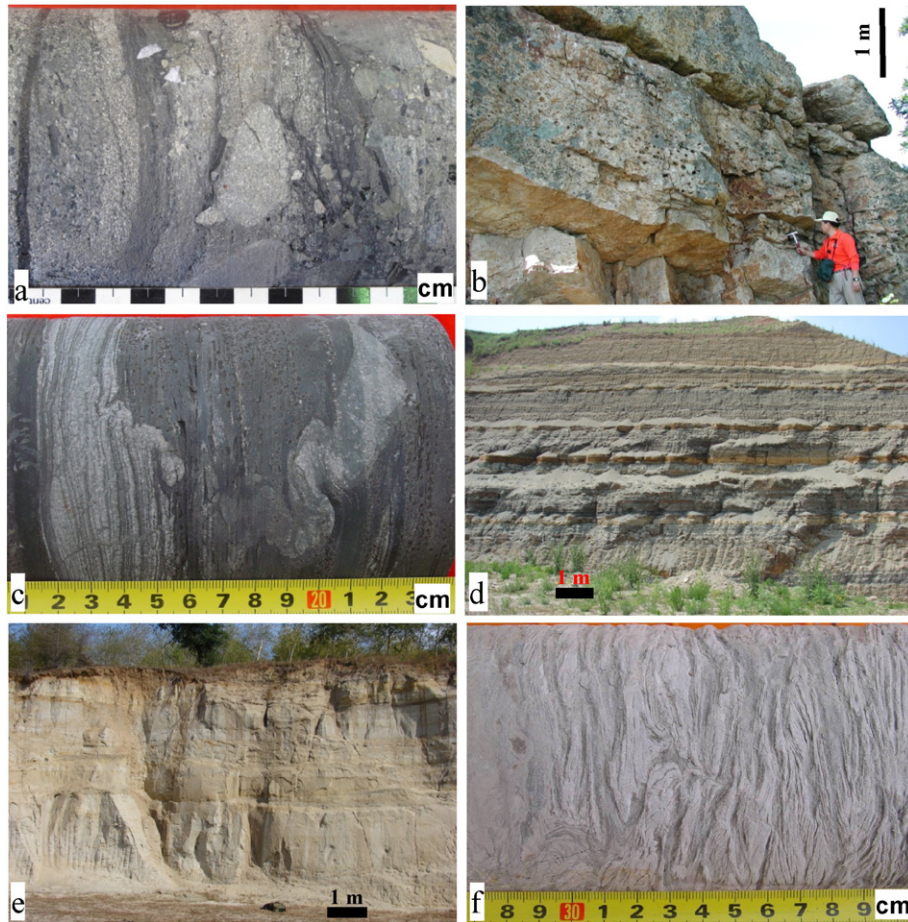


Fig. 5. Photographs showing basin fill elements of the three tectono-stratigraphic successions from syn-rift (a, b), post-rift (c, d), and structural inversion (e, f). (a) Shahezi Formation, coal-bearing dark clastic rocks from well-FS101 at a depth of 3597 m. (b) Yingcheng Formation, grayish rhyolite with elongated vesicles and flow banding from an outcrop in the southeastern SB. (c) Qingshankou Formation, ostracod-bearing dark mudstone with slump structures, related to volcanism from well-SK-1s at a depth of 1682 m. (d) Nenjiang Formation, interbedded dark mudstone and oil shale, containing ostracod-bearing limestone and dolomite concretion layers from an outcrop in the eastern SB. (e) Sifangtai Formation, grayish yellow sandstone with parallel- and cross-beddings from an outcrop in the northern SB. (f) Mingshui Formation, gray sandstone with syn-sedimentary deformation structures from well-SK-1n at a depth of 424 m. The outcrop sites are shown in Fig. 6. For the borehole locations, see Fig. 3.

Kravchinsky et al., 2002). The second one was the consequent mega-rifting on the two-sided continental margin setting of the entire region of Northeast Asia during the Late Jurassic and Early Cretaceous (Graham et al., 2001; Kirillova, 2003). The third event was the rapid subsidence and deposition, exclusively observed in the SB during the Late Cretaceous (Feng et al., 2010; Wang et al., 2013).

The closure of the Mongol–Okhotsk Ocean ensued mainly during the Jurassic but ended during the Early Cretaceous (Cogné et al., 2005; Metelkin et al., 2010; Van der Voo et al., 2015). It is generally believed that the oceanic crust was subducted to the northwest, beneath Siberia (Van der Voo et al., 2015; also note Doglioni et al., 1999a). The related Mongol–Okhotsk Collisional Belt formed after the ocean basin closure, at a distance of more than 400 km to the SB (Fig. 2). Associated with the later stage of the suturing event, large scale rifting affected the whole region of Northeast Asia during the Late Jurassic and Early Cretaceous. Hundreds of grabens and half grabens developed during that time.

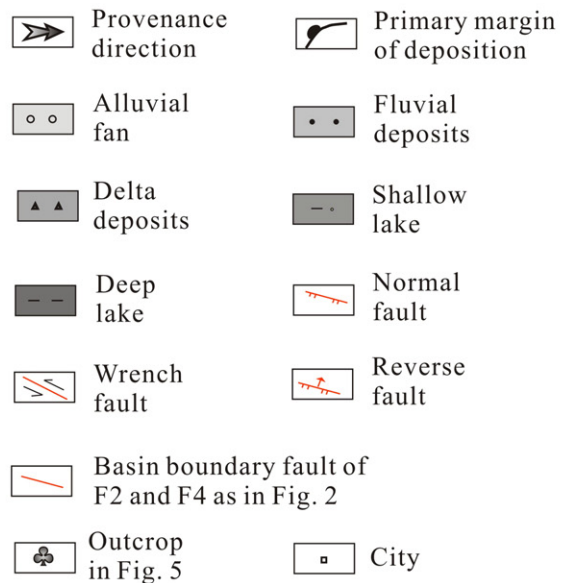
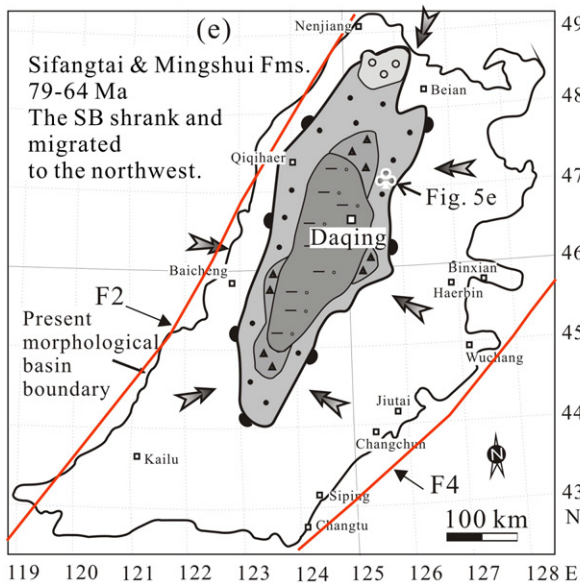
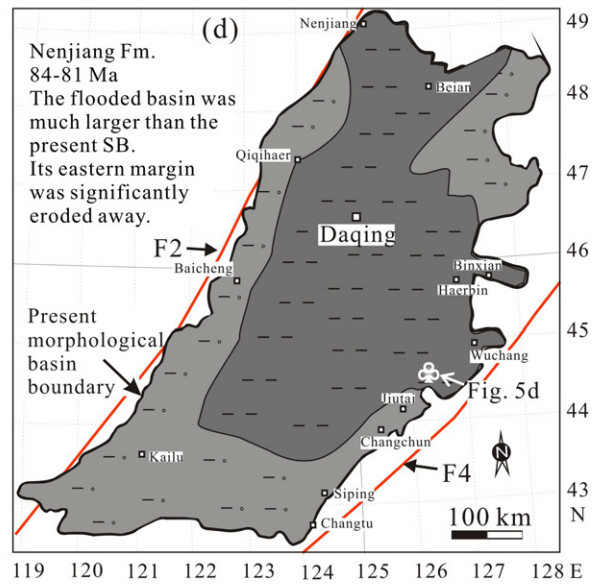
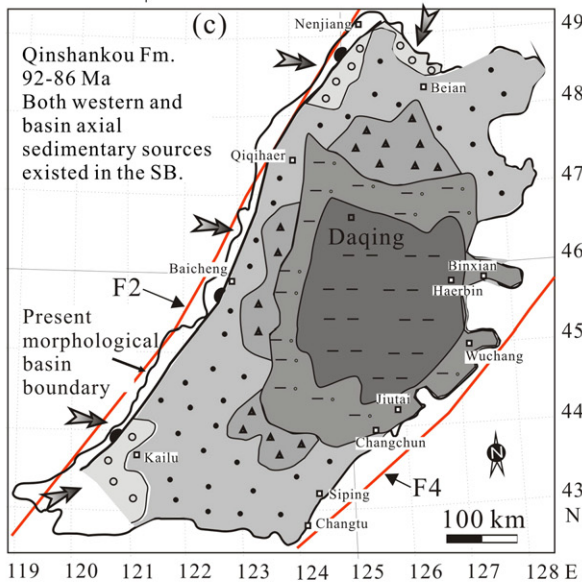
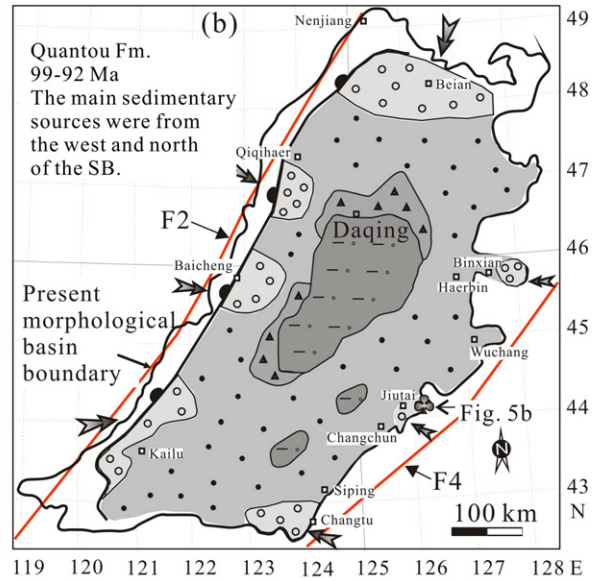
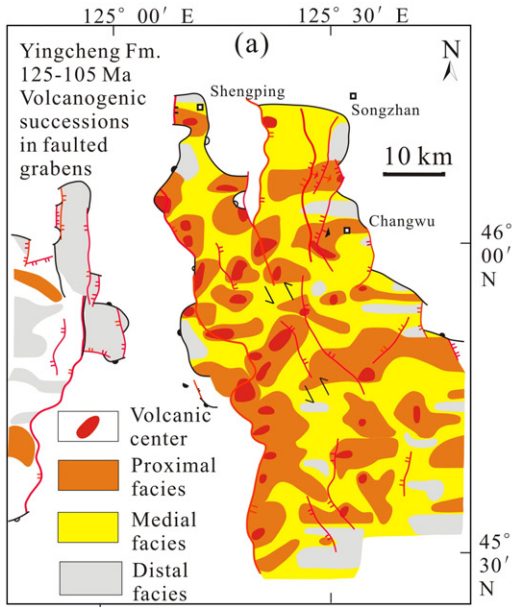
Basin-generating patterns changed significantly during the Late Cretaceous, showing very rapid subsidence and only a limited number of depocenters, unlike the previous phases of mega-rifting. The SB became the incomparably largest Upper Cretaceous basin in Northeast Asia, accommodating thousands of meters of oil-bearing sedimentary sequences (DPGC, 1993). During the mid-Cretaceous, flood basalt up to 200 m thick and dated at 88 ± 0.3 Ma (Ar–Ar method; Wang et al., 2009b), was poured out along the axis of the SB at the shallowest Moho zone of the region (Figs. 4 and 8). The basalt is characterized by

olivine-bearing mugearite, rich in Na, Al, LREE ($\sum \text{LREE}/\sum \text{HREE} = 8.0\text{--}9.7$) and LILE (e.g. U, Th, Pb, Rb, Sr and Ba) and with the δEu values ranging from 0.95 to 1.36 (Wang et al., 2009b). This flood basalt event possibly implies that the onset of a potential embryonic drift stage had been reached (Yang et al., 2004). Following the basalt eruption, marine ingression deposits accumulated during the mid-Turonian and early Campanian (Fig. 4). Consequently, the SB reached its maximum flooding phases (Qingshankou and Nenjiang Formations in Figs. 3, 6 and 7) during the mid-Cretaceous, characterized by the most rapid subsidence, fastest black shale accumulation and the largest area of deposition during the basin's evolution.

In summary, the SB was located between two active margins during the Jurassic and Cretaceous. On the Pacific side to the SE, oceanic subduction occurred under the SB and continued to this day, outlasting the westward closure of the Mongol–Okhotsk Ocean and the collision to the NW of the SB.

3.4. Cenozoic

After sedimentation reached a standstill in the SB during the mid-Danian (Fig. 4), the wide area west of eastern margin fault F4 (Figs. 2 and 3) actually ceased to accumulate any Cenozoic deposits, except for a few small scale patches of Quaternary basalts (IGS, 1991; HGS, 1993) (Fig. 3). However, both volcanism and sedimentation became active in the meantime to the east of the SB and were mainly associated with the northern branches of the giant Tanlu strike-slip fault zone, which



includes the Liaohe Basin and the Jiamusi-Yitong and Dunhua-Mishan grabens (Figs. 2 and 3). Paleogene volcanogenic successions measuring up to 7000 m in thickness formed in the Liaohe Basin, which are predominantly subaquatic eruptions (Fig. 2, e.g., LPGC, 1993; Hsiao et al., 2010). While Eocene to Oligocene successions filled the Jiamusi-Yitong Grabens (Fig. 3). Younger sediments of Oligocene–Miocene age were deposited in the Dunhua-Mishan Grabens (F5 in Fig. 3) (Sun et al., 2010; J.H. Wang et al., 2011). The typical Cenozoic basin fills in the region are interbedded with epiclastic, pyroclastic and volcanic rocks in which the share of volcanogenic components can exceed 50% of the total volume (Chen et al., 1999).

3.5. Underlying crust and mantle

The crust underlying the SB is a mosaic of different microcontinents and accreted blocks (Figs. 2, 9 and 10) that had formed by the end of the Late Permian. Since the Triassic, the whole area of the SB and its surroundings has remained continental crust. This crust, however, may have experienced lithospheric delamination (Wu et al., 2005) or decratonization (Yang et al., 2010). The depth of the Moho ranges from 29 to 34 km in the SB region and 36 to 40 km in the adjacent western mountain belt (Figs. 8 and 9). There are two significant Moho highs under the SB. They occur approximately under the basin west and beneath the eastern margin of the present SB (Fig. 9a). The top of the asthenosphere ranges from 60 to 100 km below the surface, and the highest asthenospheric dome corresponds directly to the present basin center around the city of Daqing (Fig. 9b).

It should be noticed that the Moho depth is slightly increasing beneath the SB, whereas the asthenosphere shows the classic uprise beneath the basin (Fig. 9). The two quite contrasting data set have been proved since late 1990's (Zhang et al., 1998; Karsakov and Zhao, 2001). However, the reason remains to be discussed. We put forward the idea that the Moho depth slightly increases under the SB (Fig. 9) due to the basin inversion, which should result in crustal thickening and in depressing the Moho.

The density values of the asthenosphere are generally lower than those of the overlying lithosphere mantle. But there are exceptions, associated with two fault zones of the GGT in Fig. 9b. One is in the Heihe-Hegenshan Suture Zone (F8) and the other is in the eastern boundary fault zone of the SB (F4), both of which have a denser asthenosphere of 3.237 in g/cm³ and lighter lithosphere mantle of 3.190 to 3.230 in g/cm³. It is interesting to note that there is another GGT profile (Fig. 2; called "Siberian GGT") which cuts the northern part of the Siberian Craton and is nearly parallel to and is about 900 km north to the GGT profile of the Songliao Basin (Fig. 2). In contrast to GGT of the Songliao Basin the Siberian GGT shows that the overlying lithosphere mantle is predominantly lighter than the underlying asthenosphere (Karsakov and Zhao, 2001). The significantly different characteristics between the two GGTs concerning the relative densities of lithosphere mantle and asthenosphere may be caused by an age difference of the two blocks, namely, the Siberian Craton which is a much older block than the block of the Songliao Basin. We, therefore, infer that a long-lived, "mature" block has a higher potential of involving lighter upper lithospheric mantle and denser asthenosphere.

4. Basin controlling fault systems

Two sets of NNE and NW faults represent the major controlling fault systems of the SB. The NW faults only partly control the boundaries of the Early Cretaceous grabens (Figs. 3 and 6a). The NNE faults explicitly control the distribution of the Upper Cretaceous and Paleogene

sequences and strike parallel to both the long axis of the present basin and the continental margin of North Asia (Figs. 3 and 6b–e). Faults of both sets have been long-lived lithospheric faults since the Jurassic and show multiple reactivations, including ductile shear, extension, strike-slip and compression (Sun et al., 2006, 2010). In some sections, each of the lithospheric faults may coincide with ancient suture zones between blocks at shallow depth (≤ 5 km) but separate from one another at deeper levels, as shown by F2 and F8 in Figs. 9 and 10 (Liu et al., 2011), where favorable conditions for the presence of a major lithospheric scale detachment fault exist, along and above which the SB was formed and extended (Fig. 9).

4.1. The NNE-SSW striking fault system

From west to east, this system mainly includes the Nengjiang-Balihan (F2), Basin Central (F0) and Jiamusi-Yitong faults (F4) in Fig. 3. The F2 fault developed on a Paleozoic suture belt between microplates (Han et al., 2012) and separates the present Great Xing'an Mountain from the SB to the east (Fig. 3). It cuts deeply down to the Moho and is the western boundary fault for the Late Cretaceous and Paleogene sedimentary sequences (Figs. 3 and 10).

The F0 fault is the central, axial fault of the SB. Larger grabens of the Late Jurassic and Early Cretaceous developed generally along this fault or fault zone. The thickest sediments of Late Cretaceous age, a wide Moho-break belt and a zone of Coniacian flood basalts developed along the central fault system (Figs. 3b and 8). The regional erosional surface on top of the Nenjiang Formation (K_{2n}) shows that the central fault zone corresponds to the paleo-fold ridge revealed by the seismic reflector T₀₃ (ca. 79.1 Ma, Fig. 3b). All of these aspects, as well as the Paleogene to Quaternary basalts, which occur in the northern and southern parts of the fault system (Fig. 3a), suggest a long history of fault activity since the Cretaceous.

The eastern marginal fault F4 has controlled sedimentation of both the Cretaceous in the SB and the Cenozoic in the Liaohe Graben (Figs. 1 to 3). Cenozoic olivine basalts, found along the F4 fault, revealed that the crust had been sheared to at least a depth of 70 km (Wu, 1989). As recognized by Sun et al. (2006), with regard to its tectonic history and sedimentation, the F4 fault has passed through four episodes of fault movement that have accompanied the SB's evolution. The first episode was an interval of sinistral movement that coincided with the Late Jurassic and Early Cretaceous regional mega-rifting. The second episode is characterized by sinistral transtension, occurring coevally with rapid Late Cretaceous subsidence, observed only in the SB. The third movement was compressive and is characterized by overthrusting within the fault zone. It is represented by a regional erosional surface on top of the Nenjiang Formation (ca. 79.1 Ma) (Fig. 3b) (Sun et al., 2007). The last episode was dextral strike-slip during the Cenozoic, when thick volcanogenic successions of the Paleocene to Miocene accumulated in the Liaohe Basin (LGS, 1989; Qi et al., 2008).

4.2. The NW-SE and N-S striking fault systems

These fault systems are recognized in the center of the SB. They often show cross-cutting features (Fig. 2) with the younger NNE-striking faults that are the most dominant and are approximately parallel to the continental margin in the area (Figs. 1 to 3). The Lower Cretaceous grabens, buried under the Upper Cretaceous sedimentary sequence, are generally controlled by their boundary faults, striking northwest and north-south (Figs. 3a and 6a). The NS-striking faults may become steep with nearly vertical dip angles in the deeper part towards the

Fig. 6. Basin filling trends, depocenters, and facies evolution of the SB in three tectono-stratigraphic stages: syn-rift (a), post-rift (b, c, d), and structural inversion (e). Note: (1) During the syn-rift stage there were hundreds of segmented Lower Cretaceous grabens developed in northeast Asia as partly shown in Fig. 3. In (a) typical examples of them are shown, buried deeply in the center of the SB (for location see Fig. 3); (2) The basin area should be significantly larger than that of the present SB because the eastern marginal deposits of the Qingshankou and Nenjiang Formations (c and d) have been eroded, and, thus, the deep lake deposits are exposed along the present cliffed basin margin (cf. Fig. 5d).

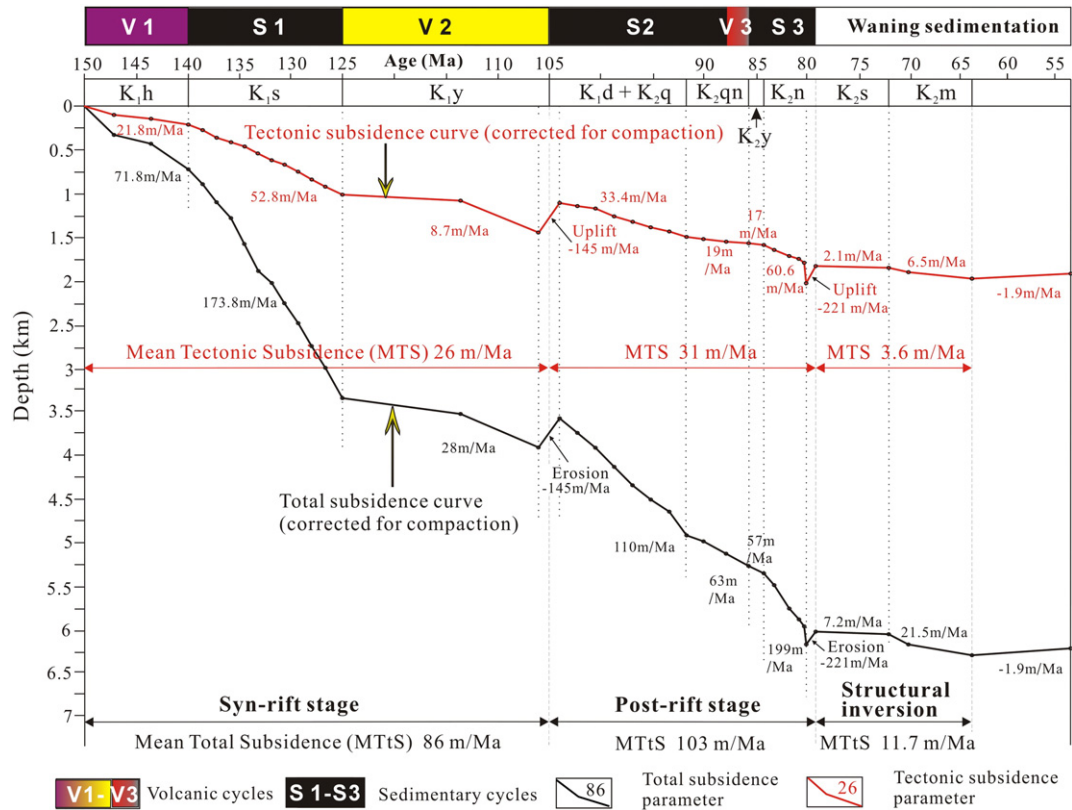


Fig. 7. Subsidence history of the SB, calculated from the SK-1s, SK-1n, and SK-2 borehole successions, co-sponsored by ICDP (International Continental Scientific Drilling Program) and China Geological Survey, showing the three tectono-stratigraphic stages of the syn-rift, post-rift and structural inversion and three volcanic-sedimentary cycles (V1-S1 to V3-S3). Tectonic subsidence indicates subsidence due to conventional extension (normal faulting) and does not include extension due to transtension. The borehole locations are shown in Fig. 3. Formation abbreviations in the third line are the same as in Fig. 3.

Moho (F0 in Fig. 9a), where they may serve as a feeder dike system for the Coniacian flood basalt along the axis of the SB (Fig. 8).

4.3. Detachment fault system

A detachment fault system may have been active beneath the SB (Fig. 9). The profound rift structures, the thinned crust and the large scale Cretaceous volcanism suggest that significant extension had affected the region that was likely related to a deep-seated detachment fault system. Metamorphic core complexes have been recognized within and around the SB, showing clear evidence of Cretaceous detachment faulting (Zhang et al., 2000; Liu et al., 2005; T. Wang et al., 2011).

Examples of detachment faults occur in the southern, northern and central parts of the SB. Ductile shear zones of the Liaonan Metamorphic Core Complex (Southeastern Liaoning Province) near the southeast margin of the SB indicate that detachment faults had frequently developed during the Early Cretaceous in the region (Liu et al., 2005). The Aptian ductile Keluo Complex, which is found near Nenjiang (Heilongjiang Province), revealed that there was a southeast directed detachment fault on the northwest margin of the SB (Liang et al., 2012). Metamorphic core complexes coupled with multilayered, low-angle ductile detachment systems were encountered in basement boreholes and 3-D seismic data in the central basement uplift of the SB (near well FS6 in Fig. 3a) (Zhang et al., 2000). There are also the Ganzhuermiao (Inner Mongolia) and the Waziju/Yiwulushan complexes (Liaoning Province) whose kinematics were studied by T. Wang et al. (2011). They are exposed around the basin margins. By means of kinematics and the distribution of Mesozoic metamorphic core complexes (MCCs) and domes with major shear sense in NE Asia, T. Wang et al. (2011) arrived at the conclusion that the SB is located in the transitional zone between domains of opposite shear sense and

placed the line between the two domains along the central basin axis. Northwest of the basin, they found an upper crustal tectonic transport to the southeast (top-to-the-SE directed, extension), which is related to the closure of the Mongol–Okhotsk Ocean, whereas to the southeast of the basin, upper crustal transport was to the northwest of the SB (top-to-the-NW, extension) and related to the subduction of Pacific lithosphere. The MCCs have $^{40}\text{Ar}/^{39}\text{Ar}$ ages of 130–110 Ma for the mylonites and U–Pb zircon ages of 150–110 Ma for the integral granitic intrusions (T. Wang et al., 2011). These ages coincide with the SB syn-rift stage of 150–105 Ma. Therefore, we infer a likely detachment fault system as depicted in Fig. 9b, which also takes into account the displaced crustal structure and the Moho breaks underneath the SB as shown in Figs. 8 and 10. In addition, we have considered the widespread Moho transition zones of Fig. 9, which are significantly thinner below the SB than in the adjacent areas, which can be attributed to ductile stretching.

5. Tectono-stratigraphy of the Songliao Basin (SB)

5.1. Volcanism and sedimentation

The fill throughout the SB is composed of three volcanic and sedimentary cycles (Figs. 4 and 7). The volcanic successions are the Berriasian andesites, Aptian–Albian rhyolites and Coniacian flood basalts. Following every volcanic episode, rapid subsidence and significant sediment accumulation occurred. The rate of total subsidence may have reached up to 199 m/Ma (Fig. 7).

There are also three major angular unconformities in the vertical succession of the SB fill (Fig. 4). They are the pre-rift erosional surface (seismic reflector T_5), the top-of-rift or break-up unconformity (T_4) and the surface that is related to the onset of the structural inversion (T_{03}) (Figs. 3b and 4). Three tectono-stratigraphic units, the syn-rift,

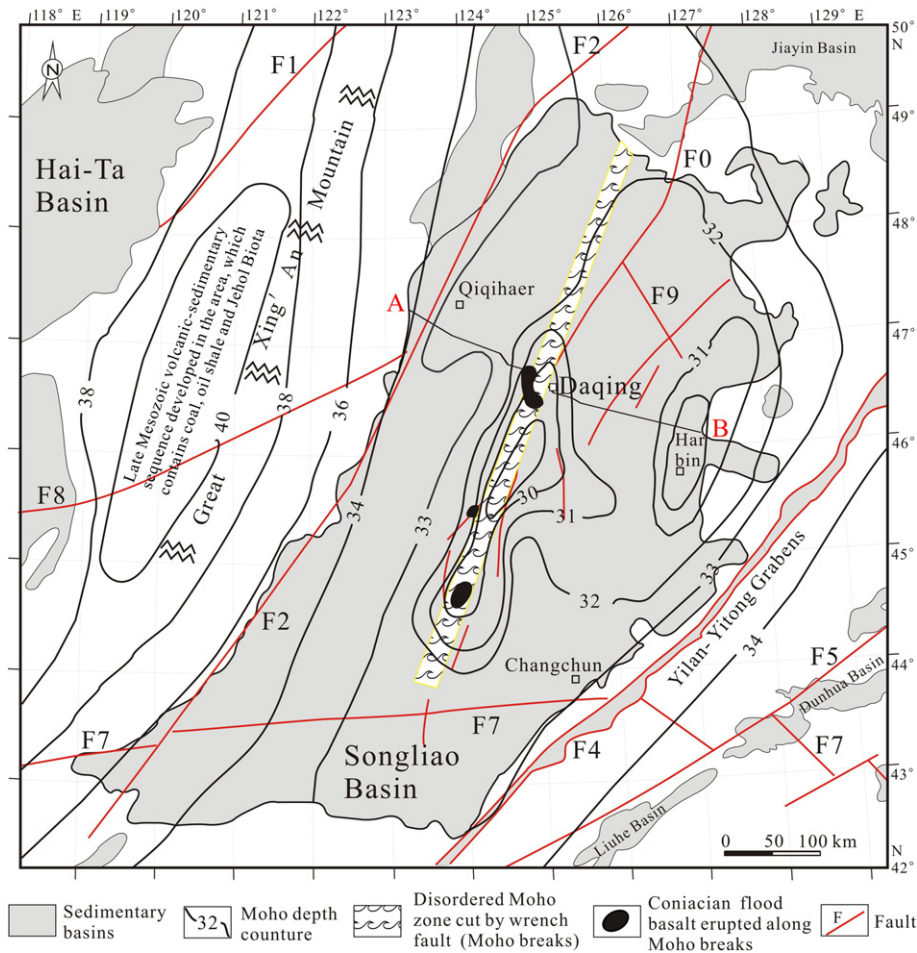


Fig. 8. Moho contour line, distribution of the Coniacian basalt, and Moho breaks in the SB, compiled from Han et al. (1988); Lu and Xia (1992); Zhang et al. (1998); Karsakov and Zhao (2001); Yang et al. (2004); Li et al. (2006) and Wang et al. (2009b).

post-rift and structural inversion sequences, are bounded by unconformities. The relationships among the tectono-stratigraphy and the volcanic-sedimentary cycles will be outlined below.

5.2. The syn-rift tectono-stratigraphy (Tithonian to mid-Albian)

This sequence is bounded by the pre-rift erosional surface (T_5) at the bottom and the top-of-rift unconformity (T_4) at the top. It is a volcanogenic succession with two volcanic cycles (Huoshiling (K_1h) and Yingcheng (K_1y) Formations), including a thick intervening sedimentary succession in the middle (Shahezi Formation, K_1s) (Figs. 4, 5 and 7). T_5 as the pre-rift erosional surface also represents the top of a pre-existing orogen in the retrobelt, having derived from subduction to the SSE (Sun et al., 2013, compare Atlantic and Mediterranean examples in Doglioni et al., 2003).

On top of the basement unconformity (reflector T_5), the basin fill begins with a fining-upward sedimentary sequence (lower Huoshiling Formation), which is composed of interbedded, dark-colored, sandstones, siltstones and mudstones that were deposited in fluvial and lacustrine environments. After these epiclastic rocks had been deposited (150–145 Ma) at a relatively low subsidence rate (72 m/Ma), the first regional volcanic eruption (upper Huoshiling Formation) started, and the volcanic activity lasted from 145 to 140 Ma. This volcanic cycle is characterized by deposition of mafic and intermediate successions (Qu et al., 2014). The middle part of the syn-rift succession is characterized by a general fining-upward, epi-/pyroclastic sedimentary sequence up to 2350 m thick (Shahezi Formation, 140–125 Ma), dominated by thick lacustrine black shale and marsh coal. There are also coarse clastic

fan-delta deposits. Following the volcanism, the subsidence rate was high (174 m/Ma). Locally, unconformably overlying the Shahezi Formation, is the Aptian volcanic succession up to more than 2000 m thick (Yingcheng Formation, 125–105 Ma), representing the largest regional volcanic episode during the Cretaceous, involving much of Northeast Asia (Wang et al., 2016). It is characterized by rhyolitic volcanic assemblages, although it can be subdivided into three lithotype members that show an upward sequence of rhyolites, coal-bearing epi-/pyroclastics and interbedded andesites and basalts (Jia et al., 2008). Both sets of volcanic rocks, Huoshiling and Yingcheng Formations, indicate an active continental margin setting, based on the element geochemistry, REE and Nd–Sr–Pb isotopic signatures (Wang et al., 2002a, 2002b, 2006). The paleoclimate was generally warm and humid for the region during the period from the Tithonian to Aptian (Huang et al., 1999).

5.3. The post-rift tectono-stratigraphy (mid-Albian to mid-Campanian)

We interpret the sequence as a post-rift unit, based on the characteristics of its enclosing sequence boundaries T_4 and T_{03} , the basin fill, overlapping the rift basin margins as well as many other faults and the sagging style in contrast to the underlying syn-rift succession (Figs. 3 and 4). This sequence is bounded by the top-of-rift unconformity (T_4) and the structural inversion surface (T_{03}) and corresponds to the sedimentary cycles 2 and 3, with an intercalation of volcanic cycle 3 (Figs. 3b, 4 and 7). Concerning both hydrocarbon source and reservoir rocks this is the most important oil and gas-bearing sequence, which is thicker than 6000 m (Gao et al., 2016). The predominant deposits are mudstone, siltstone and fine to medium-grained sandstone, composed of a

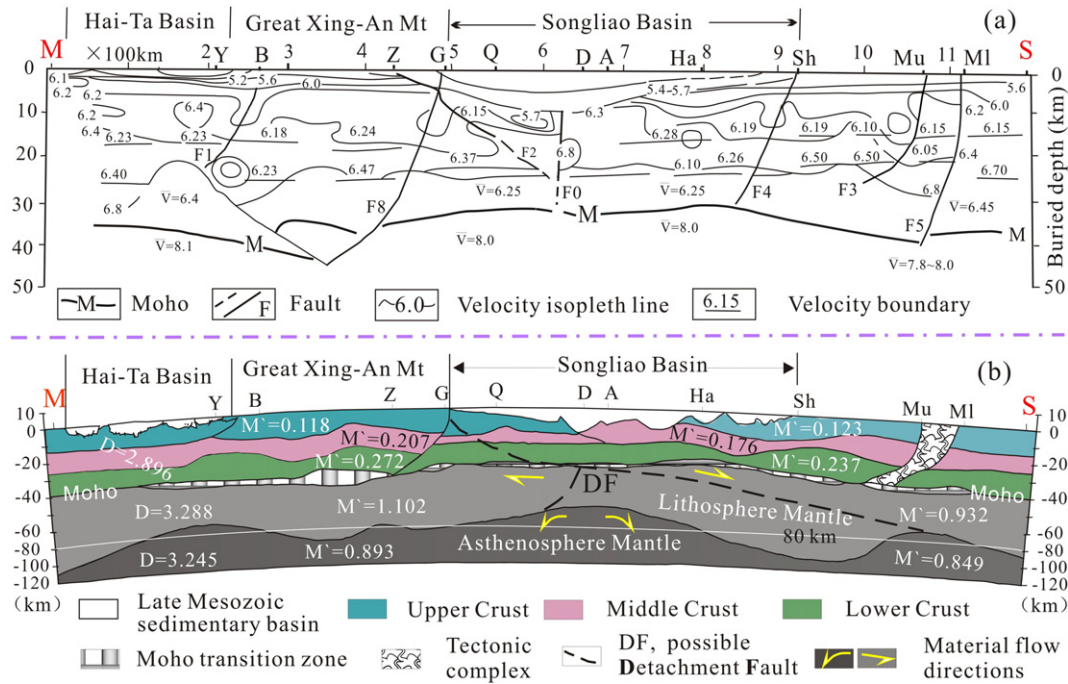


Fig. 9. Underlying crust and lithospheric and asthenospheric mantle of the SB. (a) Seismic velocity structure and geophysical boundaries of the Manzhouli-Suifenhe Global Geosciences Transect (GGT), showing features of the underlying crust in the SB (according to Yang et al. (1996)). F0 to F5 and F8 are the same as those in Figs. 2 and 3. (b) Density stratification of the crust and upper mantle along the GGT. The density values (D) of (max to min)/mean \pm SD (standard deviation) in g/cm^3 are (3.264 to 3.225)/3.245 \pm 0.013 for the asthenosphere, (3.393 to 3.190)/3.288 \pm 0.053 for the lithosphere mantle, and (2.963 to 2.837)/2.896 \pm 0.033 for the crust. The geochemical differentiation index ($M' = (\text{MgO} + \text{FeO} + \text{CaO})/(\text{SiO}_2 + \text{Al}_2\text{O}_3 + \text{Na}_2\text{O} + \text{K}_2\text{O})$) shows a significant difference between the eastern and western sides under the SB. The values in the west are typically higher (more mafic in composition) than the corresponding values in the east, except for the upper crust. The density values are from Karsakov and Zhao (2001). The material flow directions are based on regional kinematic shear sense of T. Wang et al. (2011). Others are based on Zhang et al. (1998). The detachment fault system is inferred by apparent crustal displacement, Moho breaks (Fig. 8), thinning of the Moho transition zone beneath the SB, changing mantle thickness, and the metamorphic core complexes within and around the SB (see the text for details). Cities: M—Manzhouli, Y—Yakeshi, B—Boketu, Z—Zhalantun, G—Gannan, Q—Qiqihaer, D—Daqing, A—Anda, Ha—Harbin, Sh—Shangzhi, Mu—Mudanjiang, MI—Muling, S—Suifenhe. For location of the transect see Fig. 2.

series of upward fining and coarsening cycles as well as periodic sub-cycles (Figs. 4 and 5). There are several marine intervals in the sequence, although the main sedimentary environments are fluvial, deltaic and lacustrine (Wang et al., 2013). During the marine incursions (Qingshankou and Nenjiang Formations in Figs. 4 and 6c–d), several black/dark shale layers were deposited that contain foraminifera (Xi et al., 2011). A major basalt eruption occurred during the Coniacian along the axial basin zone (Fig. 8). The thickness of the basalt succession can measure more than 200 m (upper Qingshankou Formation in Fig. 4). The basalts commonly display subaquatic eruption features such as glassy matrix and hyaloclastic textures. Pillow lavas could have been formed, but it is difficult to recognize them in cores (diameter of 9.5 cm). Geochemical signatures show that associated olivine mugearite originated from a magma chamber deeper than 60 km from an intraplate setting (Wang et al., 2009b). Along with the basalt eruptions, seismites developed with typical structures such as stepwise micro-faults, load casts and ball-and-pillow structures (Wang et al., 2010).

The post-rift stage (105–79.1 Ma) shows very fast subsidence, exclusively in the SB area. It is extraordinary that the subsidence rates were significantly higher than those of the previous rifting stage for both the total subsidence and the subsidence related to the conventional extension/normal faulting (Fig. 7). Abnormally high post-rift subsidence was recently also recognized by Li and Liu (2015). The abnormally high subsidence in the SB was coupled with deep crust faulting and basalt eruption as well as regional left-lateral movement (Yang et al., 2004; Wang et al., 2009b). In general, the thermal subsidence occurs at a low to medium rate following rifting and is significantly slower than that of the related rift stage (compare Einsele, 2000 p. 576). In a first approximation, the SB's rapid post-rift subsidence should be explained by the combination of intense thermal subsidence and

transtension, belonging to the transit fault systems of the East Asian Shear Zone (Utkin, 2013). Directly beneath the center of the SB, the present asthenosphere still shows upwelling features that coincide with thinned lithospheric mantle (Fig. 9). Similar mantle diapirs have been found to be an important mechanism to open basins in the Western Pacific (Arai et al., 2007).

5.4. The structural inversion tectono-stratigraphy (mid-Campanian to Danian)

The inversion of the SB has long been recognized (e.g., Ma et al., 1989; Song, 1997). We interpret the respective sequence as a structural inversion unit, based on the characteristics of the fold and thrust system (top of the Nenjiang Formation in Fig. 3b) that formed at the beginning of this period and the declining subsidence rate as well as the shrinkage of the depositional area (Figs. 6e and 7). The respective basin succession is situated above the major regional "compressional surface" on top of the Upper Cretaceous Nenjiang Formation (T_{03} and K_{2n} in Figs. 3b and 4). The subsidence and sedimentation rate were now markedly reduced in comparison to the two previous stages. The entire sequence is composed of a general coarsening-up cycle that consists of a series of fining-up fluvial-lake deposits for the main part and ends with alluvial fan deposits (Figs. 4 and 6e). Syn-depositional to early diagenetic deformation structures are widely developed and commonly observed (Fig. 5f), suggesting an active tectonic setting (G.D. Wang et al., 2015). The boundary between the Cretaceous and Paleogene (K/Pg) is well defined by argillaceous lake deposits in the upper part of the sequence (Fig. 4). The paleoclimate changed significantly from the previous mid-Cretaceous warm and humid climate to a more semiarid one from ca. 80.4 Ma up to the Danian (Cheng et al., 2011; Wan et al., 2013).

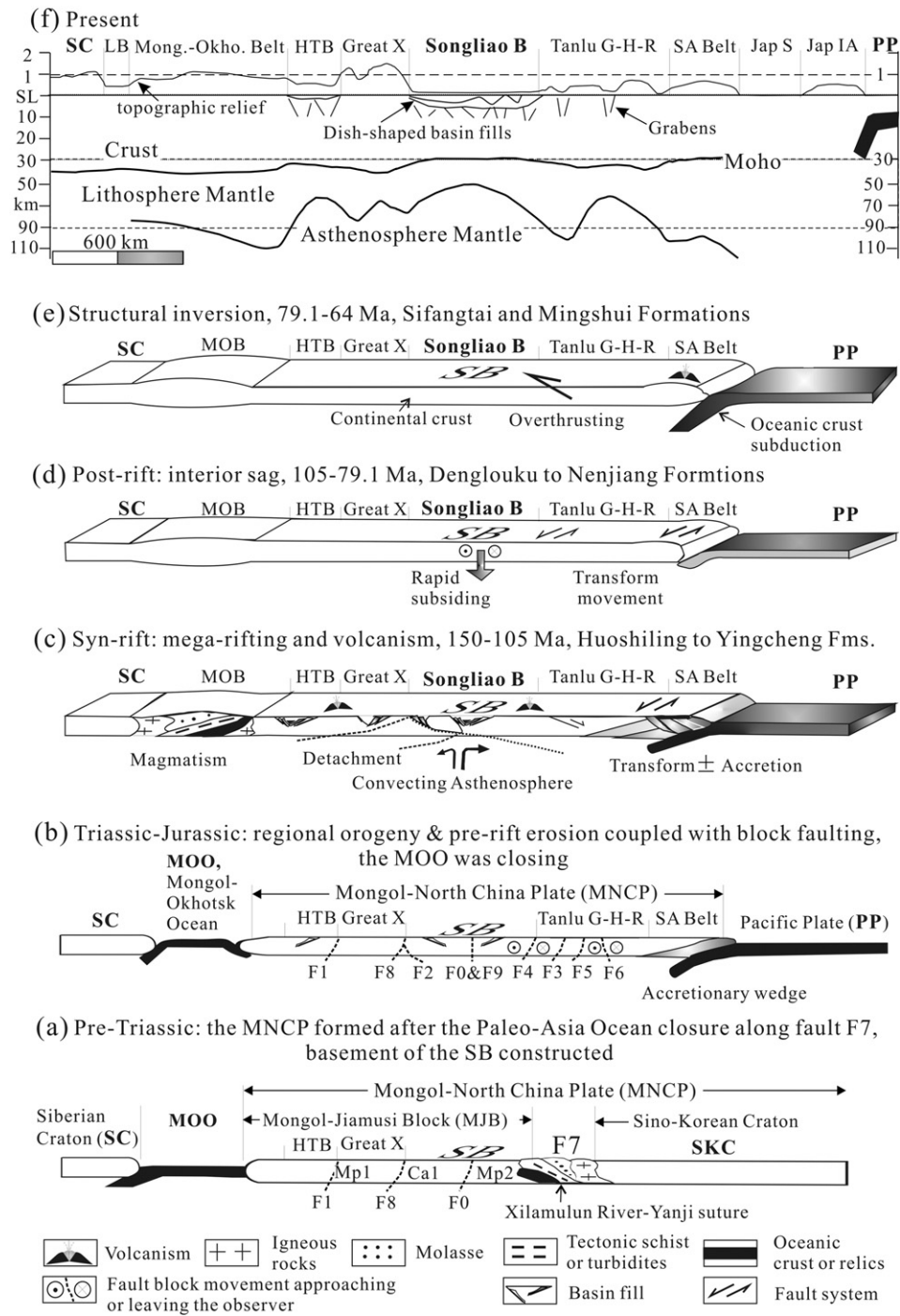


Fig. 10. The tectonic evolution of the SB and its complete geodynamic development from an active continental margin volcanic rift, via the sag basin interval to the structural inversion stage. Evolution was controlled by two-sided active continental margin tectonics of the Mongol–Okhotsk Belt, suturing in the north, and the Pacific Plate subduction in the east. SL = Sea level, SC = Siberian Craton, LB = Lake Baikal, Mong.-Okho. Belt = Mongol–Okhotsk Orogenic Belt (MOB), HTB = Hai-Ta Basin, Great X = Great Xing’An Mountain Range, Songliao B = Songliao Basin (SB), Tanlu G-H-R = Graben and horst range of the northern Tanlu Strike-Slip Fault System, SA Belt = Sikhote-Alin Orogenic Belt, Jap S = Sea of Japan, Jap IA = Japanese Island Arc, PP = Pacific Plate which is also called Izanagi (145–85 Ma) and Kula (85–70 Ma) plates during the Cretaceous (Maruyama and Send, 1986), SKC = Sino-Korean Craton. Transect lines are shown in Fig. 1. Fault and microblock abbreviations are the same as in Figs. 2 and 3. Summarized from Figs. 1 to 9 and the literature (e.g., Sun et al., 2006, 2010; Wang et al., 2007a, 2015; Kemkin, 2008; Didenko et al., 2010, 2014; Gonevchuk et al., 2010; Zybrev, 2011; Petrov et al., 2014; Khanchuk et al., 2015; Van der Voo et al., 2015). See the text for further explanations.

5.5. Basin reconfiguration

Basin reconfiguration refers to significant changes in depocenter location, basin orientation, size and shape as well as the style of basin tectonics. These aspects of the SB’s evolution are summarized in Figs. 4 and 6 and Table 1 and should be addressed with respect to the changes in

the basin dynamics. Profound basin reconfigurations occurred mainly in two phases. The first phase ensued from the syn-rift to the post-rift stage. It was characterized by a transition from mega-rifting throughout NE Asia to the accelerated, largely atetonic subsidence that was concentrated exclusively in the SB area (Figs. 1 to 3). This reconfiguration event started with a rapid uplift with an erosional rate of approximately

Table 1

Summary on the tectonic evolution of the Songliao Basin (Vol. 1 to Vol. 3 and Sed. 1 to Sed. 3 in column 2 indicate three volcanic and sedimentary cycles).

Tectonic basin cycles	Basin fill cycles	Time (Ma)	Mag-matism	Total subsidence	Tectonic Subsidence	Basin reconfiguration (A)	Basin reconfiguration (B)	Regional tectonics
Inversion	Waning sedimentation	64		11.7 m/Ma	3.6 m/Ma	A much smaller basin with depocenter migrating to the NW	Whole basin shrank; basin axis trends NNE	Compression caused by subduction of the Pacific Plate
		Structural inversion surface						
Sag	Sed. 3	79.1		103 m/Ma	31 m/Ma	Large-scale dish-shaped basin owing to rapid subsidence exclusively in the SB area	Oil & gas bearing fluvial and lake sequence with marine intervals; basin axis trends NNE	Regional compression at 79.1 Ma
	Vol. 3	88	Flood basalt					Thermal subsidence & transtension
	Sedimentary cycle 2	90.4						Top-of-rift unconformity
Rift	Volcanic cycle 2	105	Rhyolite dominant	86 m/Ma	26 m/Ma	Asymmetric graben groups, resulting from mega-rifting in the whole NE Asia	Segmented volcanogenic graben fills; basin axis trends NW, SN and NE	Transtension with sinistral strike-slip
	Sed. 1	125						Regional extension related to the active continental margins
	Vol. 1	140	Mafic dominant					
	Initial sedimentation	145						Pre-rift unconformity
Pre-rift Orogeny	Uplift & erosion	250						

– 145 m/Ma (Fig. 7), which lasted from approximately 104 Ma to 106 Ma (Meng et al., 2005). Following the uplift interval is the post-rift phase from 106 Ma to 79.1 Ma (Fig. 7). The second basin reconfiguration took place during the structural inversion process in which the SB laterally shrank. The basin center moved continuously northwestward. The onset of the waning basin development was marked by abrupt uplift and fast erosion at a rate of ca. 221 m/Ma in the mid-Campanian. The structural inversion lasted for approximately 15 Ma, from 79.1 to 64 Ma (Fig. 7) and included several fluctuations in basin size and lake level (Cheng et al., 2011).

During the two episodes of basin reconfigurations, the depositional systems and basin fill successions changed significantly. Above all, the depositional area in the region beyond the SB was continuously reduced, and the structural style changed from faulting to down-warping (Fig. 3b). During the syn-rift stage, mega-rifting involved an area of more than 4 million km² in Northeast Asia (Fig. 1). However, during the post-rift stage (105–79.1 Ma), flexural subsidence and rapid sedimentation was restricted within the SB region to approximately the present basin area (260,000 km²). During the structural inversion, sediments accumulated over an area of approximately 50,000 km², exclusively in the northwest part of the present SB (Figs. 4c and 6e).

6. Discussion

6.1. Alternating volcanic and sedimentary cycles and basin subsidence

The top of Fig. 7 indicates three volcanic cycles, each of which was followed by a sedimentary cycle. The figure also shows the three different basin stages (rift, sag and inversion) and the basin subsidence with time, expressed as tectonic subsidence (subsidence related to conventional extension/normal faulting) and as total subsidence. It is intriguing that after each volcanic cycle, the subsidence significantly increased.

The first volcanic interval occurred during the syn-rift stage of the basin. It lasted for approximately 10 Ma (Fig. 7). During this volcanic stage, a significant amount of volcanic rocks accumulated (Fig. 4), indicating that the SB was a high-volcanicity rift in the sense of Barberi et al.

(1982). The subsequent sedimentary cycle reveals a marked increase in subsidence.

The second volcanic cycle also occurred during the syn-rift stage. It lasted for 20 Ma (Fig. 7). During this cycle, many more volcanic rocks were produced than during the first cycle. The subsidence during the following second sedimentary cycle was even more pronounced (Fig. 7). This subsidence was largely post-rift-related in nature despite some conventional extension.

The third volcanic cycle was part of the late post-rift stage. It consists of only a few volcanic rocks. However, these are flood basalts that are associated with marine sediments. Even after this short volcanic interval, the subsidence rate increased (Fig. 7).

Subsidence climaxed during the latest post-rift stage, just before the beginning of the inversion stage (Fig. 7). For the remainder of the inversion stage, subsidence was markedly reduced.

Wu et al. (2005) proposed a geodynamic scenario for the widespread Early Cretaceous igneous event in Northeast China. They indicated that the granitoids resulted from the delamination of the previously thickened lithosphere caused by subduction. Crustal doming and extension corresponding to the large scale lithospheric delamination occurred between 130 and 110 Ma (Wu et al., 2011), which is a possible additional reason for the intervening volcanism and local structural collapse, associated with formation of the isolated grabens in NE Asia during the syn-rift stage, and which may have reduced the rigidity/shear strength of the lithosphere.

We are not ruling out that the roofs of shallow, depleted magma chambers may have collapsed. There is evidence for numerous volcanic breccias that formed during the rift stage (cf. Wang and Chen, 2015).

The pronounced increase in basin subsidence following all of the volcanic cycles needs to be discussed. Because volcanic rocks are basically absent during the sedimentary cycles, one may consider that regional thermal subsidence contributed to the total subsidence, in addition to loading by the basin fill. These two aspects might be insufficient to explain the rapid total subsidence. Other factors in combination with these two aspects may have been at work, including lithospheric delamination, igneous accretion, transtension and the collapse of magma chambers.

The flood basalts of the SB encouraged us to consider another potential factor for the basin's subsidence. This is the igneous accretion of dense, basic rocks below the basin by intrusion (Sparks, 1992), which implies extra cooling and thermal subsidence. Moreover, the cooling and contraction of such rock masses would also result in the formation of a high density load that would cause a flexural response of the crust (compare Einsele, 2000, p. 388) and, thus, basin subsidence, especially when considering the reduced shear strength of the lithosphere.

Sinistral wrench fault movement occurred during the syn- and post-rift stages (Figs. 3 and 8) and, therefore, also during both the volcanic and post-volcanic subsidence of Fig. 7 (cf. Sun et al., 2006; Zhang et al., 2010). Strike-slip faulting played an important role in basin generation in eastern China during the Mesozoic and Cenozoic (Deng et al., 2004). We suggest that the impressive total subsidence is related to similar deformation during the sedimentary cycles, but, in addition, the Upper Cretaceous transtension must have played a role in the post-rift subsidence (Sun et al., 2010). Subduction of oceanic lithosphere at the Pacific margin and the corresponding downward drag and asthenospheric mantle flow beneath the SB also may have contributed to the strong basin subsidence during the post-rift stage (Li and Liu, 2015).

For the inversion stage thermal cooling has to be considered in addition to down-faulting and loading by compressive tectonics.

It should be noted that our subsidence curves of ICDP wells are different from all other previous ones in that the geological time sequence has much improved for the ICDP wells (He et al., 2012; Wan et al., 2013), which has significant influence on the calculation of the subsidence history. For the Upper Cretaceous sequence, the subsidence curves of ICDP wells show very similar results to the subsidence curves calculated for other wells in the Songliao Basin because the major formations of the Upper Cretaceous are relatively uniform both in thickness and petrology and can be easily correlated basin-wide (Fig. 3b). However, for the Lower Cretaceous successions, the subsidence curves vary significantly from well to well because both thickness and lithology of the corresponding formations change significantly for different grabens. Our result based on the ICDP wells represents the subsidence history of the biggest graben in the center of the Songliao Basin during the Early Cretaceous time period.

6.2. Tectonic basin evolution: overview

The tectonic basin evolution is expressed in both the structural characteristics and basin filling styles, involving the subsidence history, basin controlling fault systems, basin fill, basin size, shape and orientation in plan view as well as tectono-stratigraphy, facies associations and event deposits in vertical succession. All of these factors display a significant difference below and above the T_4 unconformity, which suggests that it is the basin's most important stratigraphic boundary (Fig. 3). The T_4 boundary also represents the unconformity of the largest regional extent. Its position corresponds to that of break-up unconformities at the rift/passive margin transitions and coeval post-rift unconformities at the conventional rift/aulcogen transitions (compare Fig. 8 in Hoffman et al., 1974). We propose the term “top-of-rift-unconformity” for active continental margin basins.

Below the T_4 reflector are fault-bounded grabens and half grabens (Figs. 3b and 6a) with tilted blocks (Fig. 3b) and overprinted by strike-slip deformation (Zhang et al., 2010). There are obvious crustal scale master faults that controlled the formation of all of the fault basins (Figs. 3 and 10), and there is possibly a single main lithospheric scale detachment fault system (Fig. 9). In plan view, the basins are segmented small to medium scale rift groups ($n \times 100$ to ca. 10,000 km²). They are generally elongated with long axis directions trending N, NW and NE. In addition to half grabens fills, graben fills are also commonly asymmetric, due to stronger tectonic subsidence on one side of the grabens (Fig. 3b). All of the syn-rift formations are bounded by steep boundary faults.

The complexities of the SB, its backarc setting and its long history and having arrived at the basin inversion stage, make it difficult to find a perfectly fitting lithospheric shear model. We tentatively suggest the presence of an east-dipping main detachment fault beneath the SB reaching the mantle (Figs. 9b and 10) which implies simple shear and an asymmetric rift structure (Wernicke, 1981) and rules out a pure shear mechanism (McKenzie, 1978). At the lower fault termination is a respective asthenosphere high east of the SB (Figs. 9 and 10). However, this high coincides with the great Tan-Lu strike-slip fault system which may have transported this high and/or modified the deep structure. There are three other elevated parts of the asthenosphere, two to the west of the SB and one roughly coinciding with the basin (Fig. 9b). The latter in fact represents the highest rise of the asthenosphere. These four highs make it difficult to assign a specific lithospheric shear model to the SB. A model that implies a combination of pure and simple shear (Barbier et al., 1986) doesn't fit well as the main detachment would have to remain within the crust (Barbier et al., 1986).

The subbasins of the SB are asymmetric (Fig. 3). Their arrangement in the western and eastern sides (or “halves”) of the SB doesn't resemble a symmetry one could call a “mirror image” of one another as the eastern subbasins are significantly wider and deeper (Fig. 3) which may point to an east-dipping simple shear detachment in the lithosphere beneath the SB (compare Wernicke, 1981).

A second fault is present beneath the SB within lithosphere mantle. This fault is assumed to be relatively short and dipping to the west (Zheng et al., 2015) and may help explaining (to a moderate degree) the elevated asthenosphere beneath the SB (Fig. 9) despite a main simple shear detachment.

The East Pacific Rise, the Mid-Atlantic Ridge, the NW Indian Ridge as well as the Red Sea Rift and the Baikal Rift display a higher topography on their eastern sides, and it was suggested that depleted and lighter asthenosphere below these zones had shifted eastward due to a westward drift of lithosphere (Doglioni et al., 2003). Moreover, the western limbs of the Pacific, Atlantic and Indian ridges exhibit a faster and thicker lithosphere in comparison to the eastern or northeastern ones which displays a faster asthenosphere (Panza et al., 2010). These phenomena have been attributed to a combination of mantle depletion along the oceanic rifts and the westward migration of the ridges and the lithosphere relative to the mantle (Panza et al., 2010). With respect to the SB, the western margin appears to be higher elevated (Great Xinganling Mts, Figs., 3, 9 and 10) than the eastern one, though, and it is difficult to assess on which side the lithosphere is thicker as on the eastern side the Tan-Lu strike-slip fault may have transported and/or modified the lithosphere. Moreover, the young ages of both the Late Mesozoic Sikhote-Alin Orogenic Belt to the east and the Mongol-Okhotsk Orogenic Belt to the west of the SB have to be considered. These aspects hamper the application of the models of Doglioni et al. (2003) and Panza et al. (2010) without invalidating them.

Fig. 7 shows the subsidence due to conventional extension (normal faulting) and the total subsidence for the syn-rift stage. Other factors besides conventional extension may have been significant contributors to subsidence. Both types of subsidence increased after periods of volcanism. As of 105 Ma, a large scale sag basin sequence was deposited above the T_4 reflector surface. Long-term continuous subsidence was concentrated only in the SB area during this time. It lasted until 79.1 Ma. A main feature of the SB is that it is the only sizable Upper Cretaceous (105–79.1 Ma) basin in NE Asia. In fact, it is the only basin in the region that contains thick Upper Cretaceous deposits at all. At this stage, the SB was a coherent basin with a unified depocenter in which a basinward thickening sequence accumulated. Concerning the eroded eastern margin (Figs. 3b and 6c–d), the post-rift sag flooding involved a much larger area than the presently preserved basin area of 260,000 km². During the sag interval, the long axis of the SB became NNE orientated and has kept this trend without a significant change since the beginning of the post-rift stage (Fig. 6b–e). The Upper Cretaceous SB stretches parallel to the prevailing regional fault systems,

which are roughly parallel to the modern continental margin (Figs. 1 to 3). In cross-section (Fig. 3b–c), the dish-shaped sag sequence rather pinches out than terminates at the boundary faults. This sedimentary response reflects widely extending subsidence due to the flexural bending of the elastic crust (Einsele, 2000, p. 388).

During the sag stage the subsidence rate reached its maximum of 199 m/Ma following the basalt eruption (V3 in Fig. 7). Fig. 7 shows some subsidence related to conventional extension and the total subsidence for the post-rift stage, and, again, both distinguished types of subsidence increased significantly after a volcanic interval. It is intriguing that the subsidence rates during the post-rift stage (mean subsidence due to conventional extension of 31 m/Ma and total of 103 m/Ma) are significantly higher than those of the syn-rift stage (mean subsidence due to conventional extension of 26 m/Ma and total of 86 m/Ma) (Fig. 7), which contrast to the rift basin models. A “normal” rifting history will show a concavely decaying exponential subsiding curve (Einsele, 2000, p. 391–400).

After a major erosional event (T_{03} , ca. 79.1 Ma), the inverting SB changed its filling style, showing coarsening-upward, segmented, middle to small scale sag sequences that maintained a dish-shaped architecture (Fig. 3b). The general depocenters of the SB migrated continuously northwestward. The basin size was markedly reduced (Fig. 6). On top of the Mingshui Formation (mid-Danian), the SB was less than 1/5 the size of its flooding period (Figs. 3 and 6e), indicating the end of the major basin filling stage in the SB. At the same time, sedimentation and subsidence rates (mean subsidence due to the conventional extension of 4 m/Ma and total of 12 m/Ma) became much smaller, compared to those of the two previous stages (Fig. 7), showing a combined compressional flexural and sag signature if one takes into account the respective syn-depositional compressional deformation widely associated with this stage (Fig. 5f).

6.3. Causes of formation of the SB

The SB's present setting in the northeastern corner of the Mongol-North China Plate at a distance of 1500 km from the modern Pacific subduction zone is not representative of its syn- and post-rift evolution. At that time, the SB was located between two active continental margins, the Mongol–Okhotsk Suture Belt to the north and northwest and the Sikhote–Alin Accretionary Belt to the east (Fig. 10). The eastern branch of the Mongol–Okhotsk Ocean closed during the Jurassic and the corresponding migration and relative rotation of micro-blocks may have lasted to the Late Cretaceous (Cogné et al., 2005; Otofujii et al., 2006).

The Sikhote–Alin Belt evolved in two geodynamic episodes that approximately correspond to the syn- and post-rift stages of the SB. During the Valanginian–Albian, the main part of the Sikhote–Alin Belt was accreted due to northwestward subduction of the Pacific Plate to the Eurasian margin. During the Albian–Campanian, the accretionary wedge moved along the Eurasian transform margin to its present position (Didenko et al., 2014). The interaction between these two active margins provided the geodynamic scenario for the generation of the SB during the Late Mesozoic.

The plate tectonic setting and basement architecture may have played major roles in the formation of the SB, with a coinciding asthenospheric upwelling (Fig. 9b). The large scale late Mesozoic basins such SB, Hai-Ta and Sangjiang (Figs. 1 and 2) are all confined by two boundaries of crystalline cratons. They represent the northern boundary of the Sino-Korean Craton, marked by the Xilamulun River–Yanji Suture Zone and the southern boundary of the Siberian Craton, which is found at the northern Mongol–Okhotsk Suture Zone (Figs. 1 and 2). This suggests that the non-cratonized basement beneath the SB region was a favorable site for the localization and generation of the mega-rifting event, as the basement has been a zone of long-persisting “weakness” in terms of shear strength, as it was built only during the pre-Triassic.

Asthenospheric mantle upwelling is a common mechanism for generating basins on continental margins and on oceanic crust (Bally and

Snelson, 1980, their Fig. 27; Nohda, 2009; Ismail-Zadeh et al., 2013; Li and Liu, 2015), although its causal mechanism remains to be discussed (Arai et al., 2007; He et al., 2014). The backarc setting and related extension (Doglioni et al., 1999b) of the SB are held responsible for basin formation and subsidence during the rift stage and the associated calcalkaline magmatism which implies a retreating subduction hinge relative to the upper plate (e.g., Doglioni et al., 2007).

Compared to other parts of Northeast Asia, the major distinguishing features of the SB are its Upper Cretaceous fill, the highest asthenospheric uplift and the Coniacian flood basalt eruptions along an axial wrench fault system (Figs. 8 and 9). It is clear that the present asthenospheric high that is located directly under the SB represents the largest and highest asthenospheric rise in the region. Its position coincides with the larger syn-rift structures, the post-rift depocenter, the basin axis wrench fault system and the highest uplift of the structural inversion surface T_{03} (Figs. 3, 8 and 9). These aspects demonstrate the pivotal role of that the asthenospheric upwelling, in controlling basin evolution, especially in the accumulation of the Upper Cretaceous sediments. It should be noted that there are several other subordinate uplifts of the asthenosphere across the Manzhouli–Suifenhe Global Geosciences Transect (GGT in Figs. 2 and 9). They are located underneath the Hai-Ta Rift Basin of the Late Jurassic and Early Cretaceous (J_3 – K_1), the Great Xing'an Mountain Range, which is composed of J_3 – K_1 volcanic and sedimentary successions and also huge Mesozoic plutons, and the pre-Triassic suture zone of Muling (Fig. 9). These indicate that the asthenospheric flow corresponded significantly to the main crustal structures in the region.

In summary, the SB developed on a basement mosaic of structural weakness. Mega-rifting in NE Asia involved the SB and is mainly attributed to the two-sided continental margin setting, which generated a large-scale extension. As an area of high subsidence the SB coincides with the highest asthenosphere of the region. Asthenospheric upwelling coupled with regional transtensional fault movement could be a reasonable explanation for the exceptional deposition of Upper Cretaceous sediments in the SB within the compass of NE Asia.

6.4. Comparison between the SB as an active continental margin basin with aulacogens

Aulacogens develop in divergent continental margin setting (Hoffman et al., 1974; Natal'in and Sengör, 2005), commonly as failed rift arms related to triple junctions (Dewey and Burke, 1974). Their main axis usually represents a basement locus of an old collisional belt (Kiselev et al., 2012). The main features of aulacogens are rift structures and their respective sediments that are overlain by a substantial post-rift sedimentary sag sequence that extends over the limits of the inactive rift and that the basin is eventually inverted (Hoffman et al., 1974). According to Keller and Stephenson (2007), the post-rift development may record several extensional or transtensional events and at least one moderate compressional reactivation (Keller and Stephenson, 2007).

Among aulacogens, the rift cycle is often accompanied by volcanism (Kiselev et al., 2012), and the rift cycle is characterized by its alkaline geochemistry (Barberi et al., 1982; Wilson, 1989) as well as extensional faulting that is associated with terrestrial sediments (Einsele, 2000). The syntectonic sediments display abrupt thickness changes at the faults due to tectonic subsidence. The cause of rifting is either an active or inactive role of the mantle (Ziegler, 1982: mantle plume model or tensional failure model).

The SB follows a similar pattern. Between the two cratons of Sino-Korea and Siberia, the basement of the SB is composed of a series of micro-blocks that were sutured together during pre-Triassic times (Fig. 2). This “welded collage” zone, which is named the “Mongol–Jiamusi Block” (MJB), likely had a weaker shear strength than the adjacent crystalline regions, and, thus, was a favorable site for the localization of the SB rift. The rift structures of the Late Jurassic to Early Cretaceous

were predominantly formed above the MJB and involved a wide area of Northeast Asia (Figs. 1 and 2).

Rift basin development in the SB is essentially similar to that found in aulacogens. However, differences exist in the fact that rifting is related to certain subduction parameters that may cause strong to mild extension in a continental margin (e.g., Jarrard, 1986). Because the SB was situated above a downgoing oceanic slab and behind magmatic arcs (Figs. 1 and 2), the geochemical composition of the volcanic rocks displays more of a calc-alkaline signature, as they are suprasubduction-related (Wilson, 1989).

The transition from the rift to the drift stage is commonly marked by a break-up unconformity in the rift/passive margin successions. An equivalent of a break-up unconformity is also found in conventional rift/aulacogen transitions, i.e., a “post-rift unconformity”. They are time equivalent, and they are equivalent in terms of a similar stratigraphic architecture. They form when rift-faulting has ceased and atectonic subsidence allows sediments to overlap the inactive faults (Hoffman et al., 1974, stages 3 and 4 in their Fig. 3). The SB displays the same stratigraphic feature, which we refer to as a “top-of-rift unconformity” in recognition of its different setting.

The atectonic post-rift sag cycle in aulacogens is characterized by the cessation of extensional fault activity. Sedimentary rocks of terrestrial and/or shallow marine facies are draped over the rift deposits and beyond as they cover the rift shoulders and are thickest above the center of the rift, i.e., where the cooling is most pronounced (e.g., Hoffman et al., 1974). The long-lasting subsidence is controlled by the lithospheric cooling and sedimentary loading of the crust (Ziegler, 1982). Volcanic rocks are usually absent.

Overlying the SB's rift grabens and the top-of-rift unconformity is the Upper Cretaceous sedimentary sag supersequence, which rests above the region's largest uplift of asthenospheric mantle (Fig. 9b). The sag development displays differences with respect to that of aulacogens because there is still volcanic activity. Moreover, some conventional extension and some transtensional faulting have occurred. The latter was concentrated along the basin axis and was accompanied by a flood basalt eruption (Fig. 8). The basalt may be related to the asthenosphere upwelling, which in turn accelerated the basin formation (Wang et al., 2009b). The transtension along the basin axis seems to be best explained by the oblique subduction of the Pacific Plate coupled with the formation of the Sikhote-Alin accretionary wedges (compare Fitch, 1972; Woodcock, 1986; Hansen, 1992; Didenko et al., 2014).

Towards the end of the evolution of an aulacogen, compressive structural overprinting/basin inversion occurs, which may be caused by continental collision (Hoffman et al., 1974, stage 5 in their Fig. 3). Examples include the Southern Oklahoma Aulacogen and the Athapuskow Aulacogen (Hoffman et al., 1974), the Dnieper-Donets Basin (Chekunov et al., 1992; Stephenson, 1993; Stovba et al., 1996; Wilson and Lyashkevich, 1996) and the Southern Indus Basin (Zaigham and Mallick, 2000). Basin inversion due to collision will eventually affect aulacogens because they are located at a continental margin (Hoffman et al., 1974). Because such aulacogens strike more or less perpendicular (not parallel) to the continental margin (Hoffman et al., 1974), basin inversion may be relatively mild.

Postsag basin inversion also occurred in the SB. Basins of this type may be deformed more intensely in the event of a collision, as they trend parallel to a continental margin. In fact, basin inversion may also precede a collision due to a change in subduction parameters (compare Jarrard, 1986). The inversion phase is characterized by compressional reactivation of the SB during the interval 79.1–64 Ma. This is revealed by the tectonic style of uplift structures on top of the post-rift sequence (T_{03} , ca. 79.1 Ma in Fig. 3b) that deformed the sediments of Denglouku to Nenjiang Formations (Figs. 3, 4 and 6). Subsidence and sedimentation were low, and erosional surfaces frequently formed (Figs. 3b, 4a and 7). The segmented sub-basins became larger and deeper northwestward ($K_{2s} + K_2m$ and above in Fig. 3b). These aspects imply that strong compressional stress, deriving from the southeast where at work, most

likely were related to the subduction of the Pacific Plate and continental margin accretion during the Campanian (Maruyama and Send, 1986; Didenko et al., 2014).

7. Conclusions

The setting of the SB during the Late Mesozoic was that of a double-sided active continental margin between the Mongol–Okhotsk and Sikhote–Alin orogenic belts (Figs. 1 and 2). The two margins created the SB, although each may have had different impacts on the SB evolution. The northern Mongol–Okhotsk Belt played a role in establishing the basin's boundary faults (Ch. 3) and in causing upper crustal tectonic transport to the SE, towards the SB's basin axis (T. Wang et al., 2011). By contrast, the effects of the eastern active margin, where subduction of the Pacific Plate occurred with changing subduction parameters, were colossal. The effects may include most of the thermal and magmatic processes. The upwelling of the asthenosphere and extension are attributed to the subduction-related processes at this active margin (e.g., Bally and Snelson, 1980).

The basement mosaic underneath the SB is pieced together from several pre-Triassic blocks and, thus, is in a zone of “mechanical weakness”. This thermomechanically young piece of basement provided advantageous conditions for generating the SB and its different successive basin cycles. Asthenospheric upwelling coupled with detachment faulting is explicitly implicated in the formation of the SB.

Three tectonic basin cycles and filling stages can be recognized for the SB: the syn-rift (150–105 Ma), post-rift (105–79.1 Ma) and structural inversion (79.1–64 Ma). In contrast to classic rift systems, the post-rift subsidence rate is the highest during the SB evolution (Table 1). Volcanic and sedimentary sequences alternated during the syn-rift and post-rift stages. The fact that subsidence significantly increased after each volcanic interval seems to point to magmatic causes in addition to regional thermal subsidence and the load of the basin fill. These causes may include basic igneous magma accretion and the collapse of a magma chambers. During the Upper Cretaceous, subsidence must have been significantly accelerated by regional transtension. In addition, the delamination of the lithosphere could be a possible additional reason for the subsidence during the syn-rift stage. Moreover, Li and Liu (2015) have put forward the idea that anomalously strong subsidence during the post-rift stage could have been due to the subduction of oceanic lithosphere at the Pacific margin and the related downward drag and asthenospheric mantle flow beneath the SB.

Mega-rifting occurred in the whole region of NE Asia, with the SB being involved during the syn-rift stage. During the post-rift stage, the association of flood basalt eruptions and marine sediments possibly suggests the incipient formation of an embryonic ocean basin during the Coniacian, coinciding with corresponding Moho breaks. During the structural inversion stage, the basin area shrank significantly, and the depocenter(s) moved gradually northwestward. The evolution of the basin stopped by the mid-Danian, owing to southeastward compressional stress, related to the subduction of the Pacific Plate toward the Asian continent.

We consider the SB to be a complete active continental margin basin with a rift, sag and inversion basin cycle and a top-of-the-rift unconformity. From our understanding of the SB, we suggest the following general model for the active continental margin basins that are situated in a backarc.

Rift cycles in active continental margin basins are generally similar to those in conventional rifts. Differences exist in the fact that rifting depends on the subduction parameters, which may cause strong to mild extension in marginal regions (e.g., Jarrard, 1986), and that the geochemical composition of the volcanic rocks are more calc-alkaline in nature, as they are suprasubduction-related (Wilson, 1989).

Active continental margin basin(s) will eventually enter a stage of atectonic subsidence, similar to that of aulacogens. This will involve significant cooling and, thus, thermal subsidence. However, during this sag

cycle, the basin will still be near the related active continental margin, and, thus, tectonic subsidence may be accompanied with some dip-and/or strike-slip faulting, depending on the subduction parameters. Sag cycles in active continental margin basins will likely include volcanism.

Basin inversion will after all affect an active continental margin basin because it is located at the continental margin and usually strikes parallel to the continental margin. Thus, basin inversion by collision may be more intense than in the case of aulacogens, which do not tend to strike parallel to the continental margin (Hoffman et al., 1974). Moreover, basin inversion may also precede a collision due to a change in the subduction parameters (compare Jarrard, 1986).

The subsidence behavior may also differ. The subsidence curves in active continental margin basins may be quite individual and difficult to decipher due to the large number of possible causes. The SB is a two-sided active continental margin basin. However, both active sides differ as to the upper or lower plate position of the SB and as to their impact on the basin evolution. The effects of the northern/northwestern margin were modest in contrast to the immense influence of the Pacific Plate margin. The application of our model only requires settings with the presence of one Pacific Plate margin type.

Acknowledgments

This study was financially supported by the National Basic Research Program of China (973 Project) grant no. 2012CB82202 and by the National Natural Science Foundation of China (grant no. 41472304). We thank Dr. Carlo Doglioni and two anonymous referees for their constructive comments.

References

- Allen, P.A., Allen, J.R., 2005. *Basin Analysis: Principles and Applications*. Blackwell Publ., Oxford London (549 pp.).
- Arai, S., Abe, N., Ishimaru, S., 2007. Mantle peridotites from the Western Pacific. *Gondwana Res.* 11 (1–2), 180–199. <http://dx.doi.org/10.1016/j.gr.2006.04.004>.
- Bally, A.W., Snelson, S., 1980. Realms of Subsidence. In: Miall, A.D. (Ed.), *Facts and Principles of World Petroleum Occurrence*. Can. Soc. Pet. Geol. Mem. Vol. 6, pp. 9–94.
- Barberi, F., Santacroce, R., Varet, J., 1982. Chemical Aspects of Rift Magmatism. In: Pálmason, G. (Ed.), *Continental and Oceanic Rifts, Geodynamic Series 8*. Boulder Publ. Co., Washington, pp. 223–258.
- Barbier, F., Duvergé, J., Le Pichon, X., 1986. Structure profonde de la marge Nord-Gasconne. Implications sur le mécanisme de rifting et de formation de la marge continentale. *Bull. Centres Rech. Explor. Prod. Elf-Aquitaine* 10, 105–121.
- Bazhenov, M.L., Alexutin, M., Bondarenko, G.E., Sokolov, S.D., 1999. Mesozoic paleomagnetism of the Taigons Peninsula, the Sea of Okhotsk: implications to kinematics of continental and oceanic plates. *Earth Planet. Sci. Lett.* 73 (1), 113–127. [http://dx.doi.org/10.1016/S0012-821X\(99\)00214-9](http://dx.doi.org/10.1016/S0012-821X(99)00214-9).
- Bussien, D., Gombojav, N., Winkler, W., Quadt, A.V., 2011. The Mongol–Okhotsk Belt in Mongolia: an appraisal of the geodynamic development by the study of sandstone provenance and detrital zircons. *Tectonophysics* 510, 132–150. <http://dx.doi.org/10.1016/j.tecto.2011.06.024>.
- Chekunov, A.V., Garvish, V.K., Kutas, R.I., Ryabchun, L.I., 1992. Dnieper–Donets paleorift. *Tectonophysics* 208, 257–272. [http://dx.doi.org/10.1016/0040-1951\(92\)90348-a](http://dx.doi.org/10.1016/0040-1951(92)90348-a).
- Chen, Z.Y., Yan, H., Li, J.S., Zhang, G., Zhang, Z.W., Liu, B.Z., 1999. Relationship between Tertiary volcanic rocks and hydrocarbons in the Liaohe Basin, People's Republic of China. *AAPG Bull.* 83 (6), 1004–1014.
- Cheng, X.R., 1982. Situation of the Songliao Basin in the plate tectonics and its hydrocarbon occurrence. *Pet. Explor. Dev.* 9 (6), 39–48 (in Chinese with English abstract).
- Cheng, R.H., Wang, G.D., Wang, P.J., Gao, Y.F., Ren, Y.G., Wang, C.S., 2011. Centimeter-scale sedimentary sequence description of Upper Cretaceous–Lower Paleogene Mingshui Formation: lithostratigraphy, facies and cyclostratigraphy, based on the scientific drilling (SK1) borehole in the Songliao Basin. *Earth Sci. Front. (Chin. Ed.)* 18 (6), 285–328 (in Chinese with English abstract).
- Chillingarian, G.V., Wolf, K.H., 1976. *Compaction of Coarse-Grained Sediments*. Elsevier Sci. Publ. Comp., Amsterdam Oxford New York (871 pp.).
- Cogné, J.P., Kravchinsky, V.A., Halim, N., Hankard, F., 2005. Late Jurassic–Early Cretaceous closure of the Mongol–Okhotsk Ocean demonstrated by new Mesozoic palaeomagnetic results from the Trans-Baikal area (SE Siberia). *Geophys. J. Int.* 163 (2), 813–832. <http://dx.doi.org/10.1111/j.1365-246X.2005.02782.x>.
- Deng, J.F., Mo, X.X., Zhao, H.L., Wu, Z.X., Luo, Z.H., Su, S.G., 2004. A new model for the dynamic evolution of Chinese lithosphere: 'continental roots-plume tectonics'. *Earth-Sci. Rev.* 65, 223–275. <http://dx.doi.org/10.1016/j.earscirev.2003.08.001>.
- Dewey, J.F., Burke, K., 1974. Hot Spots and Continental Break-up: Implications for Collisional Orogeny. *Geology*, 2, 57–60.
- Didenko, A.N., Kaplun, V.B., Malyshev, Y.F., Shevchenko, B.F., 2010. Lithospheric structure and Mesozoic geodynamics of the eastern central Asian orogen. *Russ. Geol. Geophys.* 51 (5), 492–506. <http://dx.doi.org/10.1016/j.rgg.2010.04.006>.
- Didenko, A.N., Khanchuk, A.I., Tikhomirova, A.I., Voinova, I.P., 2014. Eastern segment of the Kiselevka–Manoma terrane (Northern Sikhote–Alin): paleomagnetism and geodynamic implications. *Russ. J. Pac. Geol.* 8 (1), 18–37. <http://dx.doi.org/10.1134/S1819714014010023>.
- Doglioni, C., Harabaglia, P., Merlini, S., Mongelli, F., Peccerillo, A., Piromallo, C., 1999a. Orogens and slabs vs. their direction of subduction. *Earth-Sci. Rev.* 45, 167–208.
- Doglioni, C., Gueguen, E., Harabaglia, P., Mongelli, F., 1999b. On the Origin of West-Directed Subduction Zones and Applications to the Western Mediterranean. In: Durand, B., Jolivet, L., Horvath, F., Séranne, M. (Eds.), *The Mediterranean Basins: Tertiary Extension within the Alpine Orogen*. Geological Society, London, Spec. Publ. Vol. 156, pp. 541–561.
- Doglioni, C., Carminati, E., Bonatti, E., 2003. Rift asymmetry and continental uplift. *Tectonics* 22, 1024–1031. <http://dx.doi.org/10.1029/2002TC001459>.
- Doglioni, C., Carminati, E., Cuffaro, M., Scrocca, D., 2007. Subduction kinematics and dynamic constraints. *Earth-Sci. Rev.* 83, 125–175.
- DPGC (Daqing Petroleum Geology Committee), 1993. *Petroleum Geology of China vol. 2. Pet. Indust. Press, Beijing* (875 pp., in Chinese).
- Einsele, G., 2000. *Sedimentary Basins: Evolution, Facies, and Sediment Budget*. Springer-Verlag, Berlin Heidelberg New York (792 pp. <http://link.springer.com/book/10.1007%2F978-3-662-04029-4>).
- Feng, Z.Q., Jia, C.Z., Xie, X.N., Zhang, S., Feng, Z.H., Timothy, A.C., 2010. Tectonostratigraphic units and stratigraphic sequences of the nonmarine Songliao Basin, Northeast China. *Basin Res.* 22 (1), 79–95. <http://dx.doi.org/10.1111/j.1365-2117.2009.00445.x>.
- Fitch, T.J., 1972. Plate convergence, transcurrent faults, and internal deformation adjacent to Southeast Asia and the Western Pacific. *J. Geophys. Res.* 77 (23), 4432–4460. <http://dx.doi.org/10.1029/jb077i023p04432>.
- Gao, Y.F., Wang, P.J., Wan, X.Q., Wu, H.Y., Wang, S.X., Liang, W.L., 2016. High resolution continuous sedimentary records of Upper Cretaceous obtained from the continental drilling (SK-1) borehole in Songliao Basin: Nenjiang Formation. *Geosci. Front.* 7, 19–37 (in press).
- Gonevchuk, V.G., Gonevchuk, G.A., Korostelev, P.G., Semenyaka, B.I., Seltmann, R., 2010. Tin deposits of the Sikhote–Alin and adjacent areas (Russian Far East) and their magmatic association. *Aust. J. Earth Sci.* 57 (6), 777–802. <http://dx.doi.org/10.1080/08120099.2010.503993>.
- Graham, S.A., Hendrix, M.S., Johnson, C.L., Badamgarav, D., Badarch, G., Amory, J., Porter, M., Barsbold, R., Webb, L.E., Hacker, B.R., 2001. Sedimentary record and tectonic implications of Mesozoic rifting in southeast Mongolia. *Geol. Soc. Am. Bull.* 113 (12), 1560–1579. [http://dx.doi.org/10.1130/0016-7606\(2001\)113<1560:sratio>2.0.co;2](http://dx.doi.org/10.1130/0016-7606(2001)113<1560:sratio>2.0.co;2).
- Han, G.L., Zhao, H.T., Bian, W., 1988. Relationship between the injected basalt in Qingshankou Formation and oil/gas in Zhongyang depression, Songliao Basin. *Exp. Pet. Geol.* 10 (3), 248–255 (in Chinese with English abstract).
- Han, G.Q., Liu, Y.J., Neubauer, F., Genser, J., Zou, Y.X., Li, W., Liang, C.Y., 2012. Characteristics, timing, and offsets of the middle-southern segment of the western boundary strike-slip fault of the Songliao Basin in Northeast China. *Sci. China Earth Sci.* 55 (3), 464–475. <http://dx.doi.org/10.1007/s11430-012-4362-y>.
- Hansen, V.L., 1992. The Importance of Subduction-Related Margin-Parallel Shear Zones along Transpressional Convergent Plate Margins. In: Bartholomew, M.J., Hyndman, D.W., Mogk, D.W., Mason, R. (Eds.), *Characterization and Comparison of Ancient and Mesozoic Continental Margins, Proceedings of the 8th International Conference on Basement Tectonics, Butte, Montana, 1988, Basement Tectonics, 8*. Kluwer Academic Publishers, Dordrecht, pp. 51–65.
- He, H.Y., Deng, C.L., Wang, P.J., Pan, Y.X., Zhu, R.X., 2012. Toward age determination of the termination of the Cretaceous Normal Superchron. *Geochem. Geophys. Geosyst.* 13 (1), 1–20. <http://dx.doi.org/10.1029/2011GC003901>.
- He, C.S., Dong, S.W., Chen, X.H., Santosh, M., Niu, S.Y., 2014. Seismic evidence for plume-induced rifting in the Songliao Basin of Northeast China. *Tectonophysics* 627, 171–181. <http://dx.doi.org/10.1016/j.tecto.2013.07.015>.
- HGS (Heilongjiang Geological Survey), 1993. *Regional Geology of Heilongjiang Province of China*. Geol. Publ. House, Beijing (734 pp., in Chinese).
- Hoffman, P., Dewey, J.F., Burke, K., 1974. Aulacogens and their Genetic Relation to Geosynclines, with a Proterozoic Example from Great Slave Lake, Canada. In: Dott, R.J., Shaver, R.H. (Eds.), *Modern and Ancient Geosynclinal Sedimentation*. SEPM Spec. Publ. 19, Tulsa, Oklahoma, pp. 38–55.
- Hsiao, L.Y., Graham, S.A., Tilander, N., 2010. Stratigraphy and sedimentation in a rift basin modified by synchronous strike-slip deformation: southern Xialiao basin, Bohai, offshore China. *Basin Res.* 22 (1), 61–78. <http://dx.doi.org/10.1111/j.1365-2117.2009.00449.x>.
- Huang, Q.H., Zheng, Y.L., Yang, M.J., Li, X.J., Han, M.X., Chen, C.R., 1999. On the Cretaceous paleoclimate in the Songliao Basin. *Acta Micropalaeontol. Sin.* 16 (1), 95–103 (in Chinese with English abstract).
- IGS (Inner-Mongolia Geological Survey), 1991. *Regional Geology of Inner-Mongolia Autonomous Region of China*. Geol. Publ. House, Beijing (725 pp., in Chinese).
- Ismail-Zadeh, A., Honda, S., Tsepelov, I., 2013. Linking mantle upwelling with the lithosphere decent and the Japan Sea evolution: a hypothesis. *Sci. Rep.* 3 (1137), 1–8. <http://dx.doi.org/10.1038/srep01137>.
- Itoh, Y., Uno, K., Arato, H., 2006. Seismic evidence of divergent rifting and subsequent deformation in the southern Japan Sea, and a Cenozoic tectonic synthesis of the eastern Eurasian margin. *J. Asian Earth Sci.* 27 (6), 933–942. <http://dx.doi.org/10.1016/j.jseaes.2005.09.008>.
- Jarrard, R.D., 1986. Relations among subduction parameters. *Rev. Geophys.* 24 (2), 217–284. <http://dx.doi.org/10.1029/rg024i002p0217>.
- JGS (Jilin Geological Survey), 1988. *Regional Geology of Jilin Province of China*. Geol. Publ. House, Beijing (698 pp., in Chinese).

- Jia, J.T., Wang, P.J., Wan, X.Q., 2008. Chronostratigraphy of the Yingcheng Formation in the Songliao Basin, Cretaceous, NE China. *Geol. Rev.* 54 (4), 439–448 (in Chinese with English abstract).
- Karsakov, L.P., Zhao, C.J. (Eds.), 2001. Tectonic Map of the Central Asia-Pacific Belts Junction Area, Scale 1:1,500,000. Compiled and designed by Yu. A. Kosygin Institute of Tectonics and Geophysics, Far Eastern Branch of Russian Academy of Sciences and Shengyang Institute of Geology and Mineral Resources of China Geological Survey. Printed at 65 Kim Yu Chen St., Khabarovsk, 680000.
- Keller, G.R., Stephenson, R.A., 2007. The Southern Oklahoma and Dnieper-Donets aulacogens: a comparative analysis. *Geol. Soc. Am. Mem.* 200, 127–143. [http://dx.doi.org/10.1130/2007.1200\(08\)](http://dx.doi.org/10.1130/2007.1200(08)).
- Kelty, T.K., Yin, A., Dash, B., Gehrels, G.E., Ribeiro, A.E., 2008. Detrital-zircon geochronology of Paleozoic sedimentary rocks in the Hangay-Hentey basin, north-central Mongolia: implications for the tectonic evolution of the Mongol-Okhotsk Ocean in central Asia. *Tectonophysics* 451, 290–311. <http://dx.doi.org/10.1016/j.tecto.2007.11.052>.
- Kemkin, I.V., 2008. Structure of terranes in a Jurassic accretionary prism in the Sikhote-Alin-Amur area: implications for the Jurassic geodynamic history of the Asian eastern margin. *Russ. Geol. Geophys.* 49 (10), 759–770. <http://dx.doi.org/10.1016/j.rgg.2007.12.014>.
- Khanchuk, A.I., Didenko, A.N., Popoko, L.I., Sorokin, A.A., Shevchenko, B.F., 2015. Structure and Evolution of the Mongol-Okhotsk Orogenic Belt. In: Kröner, A. (Ed.), *The Central Asia Orogenic Belt-Geology, Evolution, Tectonics, and Models*. Borntraeger Sci. Publ., Stuttgart, pp. 211–234.
- Kirillova, G.L., 2003. Late Mesozoic–Cenozoic sedimentary basins of active continental margin of Southeast Russia: paleogeography, tectonics, and coal–oil–gas presence. *Mar. Pet. Geol.* 20 (3), 385–397. [http://dx.doi.org/10.1016/S0264-8172\(03\)00046-1](http://dx.doi.org/10.1016/S0264-8172(03)00046-1).
- Kiselev, A.I., Ernst, R.E., Yarmolyuk, V.V., Egorov, K.N., 2012. Radiating rifts and dyke swarms of the middle Paleozoic Yakutsk plume of Eastern Siberian Craton. *J. Asian Earth Sci.* 45, 1–16. <http://dx.doi.org/10.1016/j.jseas.2011.09.004>.
- Kravchinsky, V.A., Cogné, J.P., Harbert, W.P., Kuzmin, M.I., 2002. Evolution of the Mongol-Okhotsk Ocean as constrained by new palaeomagnetic data from the Mongol-Okhotsk suture zone, Siberia. *Geophys. J. Int.* 148 (1), 34–57. <http://dx.doi.org/10.1046/j.1365-246x.2002.01557.x>.
- Kumar, P., Yuan, X.H., Kumar, M.R., Kind, R., Li, X.Q., Chadha, R.K., 2007. The rapid drift of the Indian tectonic plate. *Nature* 449 (7164), 894–897. <http://dx.doi.org/10.1038/nature06214>.
- Lee, Y.S., Ishikawa, N., Kim, W.K., 1999. Paleomagnetism of Tertiary rocks on the Korean Peninsula: tectonic implications for the opening of the East Sea (Sea of Japan). *Tectonophysics* 304 (1–2), 131–149. [http://dx.doi.org/10.1016/S0040-1951\(98\)00270-4](http://dx.doi.org/10.1016/S0040-1951(98)00270-4).
- LGS (Liaoning Geological Survey), 1989. *Regional Geology of Liaoning Province of China*. Geol. Publ. House, Beijing (856 pp., in Chinese).
- Li, J.Y., 2006. Permian geodynamic setting of Northeast China and adjacent regions: closure of the Paleo-Asian Ocean and subduction of the Paleo-Pacific Plate. *J. Asian Earth Sci.* 26 (3–4), 207–224. <http://dx.doi.org/10.1016/j.jseas.2005.09.001>.
- Li, C., Liu, S.F., 2015. Cretaceous anomalous subsidence and its response to dynamic topography in the Songliao Basin, Northeast China. *J. Asian Earth Sci.* 109, 86–99. <http://dx.doi.org/10.1016/j.jseas.2015.04.045>.
- Li, D.S., Jiang, R.Q., Katz, B.J., 1995. Petroleum Generation in the Non-Marine Qingshankou Formation (Lower Cretaceous), Songliao Basin, China. In: Katz, B.J. (Ed.), *Petroleum Source Rocks*. Springer, Berlin Heidelberg, pp. 131–148. http://dx.doi.org/10.1007/978-3-642-78911-3_8.
- Li, S.L., Mooney, W.D., Fan, J.C., 2006. Crustal structure of mainland China from deep seismic sounding data. *Tectonophysics* 420 (1–2), 239–252. <http://dx.doi.org/10.1016/j.tecto.2006.01.026>.
- Li, S.Z., Zhao, G.C., Dai, L.M., Zhou, L.H., Liu, X., Suo, Y.H., Santosh, M., 2012. Cenozoic faulting of the Bohai Bay Basin and its bearing on the destruction of the eastern North China Craton. *J. Asian Earth Sci.* 47, 80–93. <http://dx.doi.org/10.1016/j.jseas.2011.06.011>.
- Liang, C.Y., Liu, Y.J., Li, W., Han, G.Q., Wen, Q.B., Neubauer, F., 2012. Uplift age of Keluo complex at Nenjiang area, Heilongjiang Province. *Chin. J. Geol.* 47 (2), 360–375 (in Chinese with English abstract).
- Liu, J.Q., Han, J.T., Fyfe, W.S., 2001. Cenozoic episodic volcanism and continental rifting in northeast China and possible link to Japan Sea development as revealed from K–Ar geochronology. *Tectonophysics* 339 (3), 385–401. [http://dx.doi.org/10.1016/S0040-1951\(01\)00132-9](http://dx.doi.org/10.1016/S0040-1951(01)00132-9).
- Liu, J.L., Gregory, A.D., Lin, Z.Y., Wu, F.Y., 2005. The Liaonan metamorphic core complex, Southeastern Liaoning Province, North China: a likely contributor to Cretaceous rotation of Eastern Liaoning, Korea and contiguous areas. *Tectonophysics* 407 (1), 65–80. <http://dx.doi.org/10.1016/j.tecto.2005.07.001>.
- Liu, C.Y., Zhao, H.G., Zhang, C., Wang, J.Q., 2009. The important turning period of evolution in the Tibet-Himalayan tectonic domain. *Earth Sci. Front. (Chin. Ed.)* 16 (4), 1–12 (in Chinese with English abstract).
- Liu, C., Yang, B.J., Wang, Z.G., Wang, D., Feng, X., Lu, Q., Liu, Y., Wang, S.Y., 2011. The deep structure of the western boundary belt of the Songliao Basin: the geoelectric evidence. *Chin. J. Geophys.* 54 (2). <http://dx.doi.org/10.3969/j.issn.0001-5733.2011.02.016> (in Chinese with English abstract, 410–406).
- LPGC (Liaohu Petroleum Geology Committee), 1993. *Petroleum Geology of China vol. 3*. Pet. Indust. Press, Beijing (550 pp., in Chinese).
- Lu, Z.X., Xia, H.K., 1992. Geotraverse from Inner Mongolia Dongwuqi to Liaoning Donggou, China (Map & Guidebook). *Earthquake Press, Beijing* (59 pp., in Chinese).
- Ma, L., Yang, J.L., Ding, Z.Y., 1989. Songliao Basin: An Intracratonic Continental Sedimentary Basin of Combination Type. In: Zhu, X. (Ed.), *Chinese Sedimentary Basins*. Elsevier Sci. Publ., Amsterdam, Netherlands, pp. 77–87.
- Maruyama, S., Seno, T., 1986. Orogeny and relative plate motions: example of the Japanese islands. *Tectonophysics* 127 (3), 305–329. [http://dx.doi.org/10.1016/0040-1951\(86\)90067-3](http://dx.doi.org/10.1016/0040-1951(86)90067-3).
- McKenzie, D., 1978. Some remarks on the development of sedimentary basins. *Earth Planet. Sci. Lett.* 40, 25–32.
- Meng, Q.A., Wang, P.J., Yang, B.J., Cheng, R.H., 2005. Geological signatures of sequence boundary of the Songliao Basin: new interpretation and their relation to gas accumulation. *Geol. Rev.* 51 (1), 46–54 (in Chinese with English abstract).
- Metelkin, D.V., Vernikovskiy, V.A., Kazansky, A.Y., Wingate, M.T.D., 2010. Late Mesozoic tectonics of Central Asia based on paleomagnetic evidence. *Gondwana Res.* 18 (2–3), 400–419. <http://dx.doi.org/10.1016/j.jgr.2009.12.008>.
- Natalin, B.A., Sengör, A.M.C., 2005. Late Palaeozoic to Triassic evolution of the Turan and Scythian platforms: the pre-history of the Palaeo-Tethyan closure. *Tectonophysics* 404 (3–4), 175–202. <http://dx.doi.org/10.1016/j.tecto.2005.04.011>.
- Nohda, S., 2009. Formation of the Japan Sea basin: reassessment from Ar–Ar ages and Nd–Sr isotopic data of basement basalts of the Japan Sea and adjacent regions. *J. Asian Earth Sci.* 34 (5), 599–609. <http://dx.doi.org/10.1016/j.jseas.2008.08.003>.
- Otofuji, Y.I., Miura, D., Takaba, K., Takemoto, K., Narumoto, K., Zaman, H., Inokuchi, H., Kulnich, R.G., Zimin, P.S., Sakhno, V.G., 2006. Counter-clockwise rotation of the eastern part of the Mongolia block: Early Cretaceous palaeomagnetic results from Bikin, Far Eastern Russia. *Geophys. J. Int.* 164 (1), 15–24. <http://dx.doi.org/10.1111/j.1365-246x.2005.02790.x>.
- Panza, G., Doglioni, C., Levshin, A., 2010. Asymmetric ocean basins. *Geology* 38, 59–62.
- Peng, P., Zhai, M.G., Guo, J.H., Zhang, H.F., Zhang, Y.B., 2008. Petrogenesis of Triassic post-collisional syenite plutons in the Sino-Korean craton: an example from North Korea. *Geol. Mag.* 145 (5), 637–647. <http://dx.doi.org/10.1017/S0016756808005037>.
- Petit, C., Déverchère, J., 2006. Structure and evolution of the Baikal rift: a synthesis. *Geochim. Geophys. Geosyst.* 7 (11), Q11016. <http://dx.doi.org/10.1029/2006gc001265>.
- Petrov, O.V., Leonov, Yu.G., Pospelov, I.I. (Eds.), 2014. Tectonics of Northern, Central and Eastern Asia: Tectonic map at scale 1:2,500,000 and explanatory note. VSEGEI Printing House, St. Petersburg (122 pp.).
- Qi, J.F., Zhou, X.H., Deng, R.J., Zhang, K.X., 2008. Structural characteristics of the Tan-Lu fault zone in Cenozoic basins offshore the Bohai Sea. *Sci. China Ser. D Earth Sci.* 51 (2), 20–31. <http://dx.doi.org/10.1007/s11430-008-6013-x>.
- Qu, X.J., Wang, P.J., Yao, R.S., Gao, Y.F., Bai, B., 2014. Stratigraphical sequence and regional correlation of Huoshiling Formation in southern Songliao Basin. *J. Cent. S. Univ. (Sci. Technol.)* 45 (8), 2716–2727 (in Chinese with English abstract).
- Ramos, V.A., 2010. The tectonic regime along the Andes: present-day and Mesozoic regimes. *Geol. J.* 45 (1), 2–25. <http://dx.doi.org/10.1002/gj.1193>.
- Ren, J.Y., Tamaki, K., Li, S.T., Zhang, J.X., 2002. Late Mesozoic and Cenozoic rifting and its dynamic setting in Eastern China and adjacent areas. *Tectonophysics* 344 (3), 175–205. [http://dx.doi.org/10.1016/S0040-1951\(01\)00271-2](http://dx.doi.org/10.1016/S0040-1951(01)00271-2).
- Ren, J.S., Niu, B.G., Wang, J., Jin, X.C., Xie, L.Z., 2013. International geological map of Asia, 1: 5000000, Institute of Geology, Chinese Academy of Geological Sciences. Geol. Publ. House, Beijing.
- Rieke, H.H., Chillingarier, G.Y., 1974. *Compaction of Argillaceous Sediments*. Elsevier Sci. Publ. Co., Amsterdam London New York (424 pp.).
- Soloviev, A., Garver, J.I., Ledneva, G., 2006. Cretaceous accretionary complex related to Okhotsk–Chukotka Subduction, Omgon Range, Western Kamchatka, Russian Far East. *J. Asian Earth Sci.* 27 (4), 437–453. <http://dx.doi.org/10.1016/j.jseas.2005.04.009>.
- Song, T., 1997. Inversion styles in the Songliao basin (northeast China) and estimation of the degree of inversion. *Tectonophysics* 283 (1), 173–188. [http://dx.doi.org/10.1016/S0040-1951\(97\)00147-9](http://dx.doi.org/10.1016/S0040-1951(97)00147-9).
- Sparks, S.J., 1992. Magma Generation in the Earth. In: Brown, G.C., Hawkesworth, C.J., Wilson, R.C.L. (Eds.), *Understanding the Earth. A New Synthesis*. Cambridge Univ. Press, pp. 91–114.
- Stepashko, A.A., 2006. The Cretaceous dynamics of the Pacific Plate and stages of magmatic activity in northeastern Asia. *Geotectonics* 40 (3), 225–235. <http://dx.doi.org/10.1134/S001685210603006x>.
- Stephenson, R.A., 1993. Continental rift development in Precambrian and Phanerozoic Europe: Europrobe and the Dnieper-Donets Rift and Polish Trough basins. *Sediment. Geol.* 86 (1), 159–175. [http://dx.doi.org/10.1016/0037-0738\(93\)90138-u](http://dx.doi.org/10.1016/0037-0738(93)90138-u).
- Stovba, S., Stephenson, R.A., Kivshik, M., 1996. Structural features and evolution of the Dniepr-Donets Basin, Ukraine, from regional seismic reflection profiles. *Tectonophysics* 268 (1), 127–147. [http://dx.doi.org/10.1016/S0040-1951\(96\)00222-3](http://dx.doi.org/10.1016/S0040-1951(96)00222-3).
- Sun, D.Y., Wu, F.Y., Gao, S., Lu, X.P., 2005. Confirmation of two episodes of A-type granite emplacement during Late Triassic and Early Jurassic in the central Jilin Province, and their constraints on the structural pattern of eastern Jilin–Heilongjiang area, China. *Earth Sci. Front. (Chin. Ed.)* 12 (2), 263–275 (in Chinese with English abstract).
- Sun, X.M., Long, S.X., Zhang, M.S., Liu, X.Y., Hao, F.J., 2006. Discovery and timing of major thrust belt in Jiamusi–Yitong fault zone. *Oil Gas Geol.* 27 (5), 637–643 (in Chinese with English abstract).
- Sun, X.M., Zhu, D.F., Zheng, C.Q., Shan, X.L., Cheng, R.H., Sun, Q.C., 2007. Feature, epoch and reservoir significance of the Mesozoic faults at the eastern margin of the Songliao Basin. *J. Jilin Univ. (Earth Sci. Ed.)* 37 (6), 1055–1063 (in Chinese with English abstract).
- Sun, X.M., Wang, S.Q., Wang, Y.D., Du, J.Y., Xu, Q.W., 2010. The structural feature and evolutionary series in the northern segment of Tancheng-Lujiang fault zone. *Acta Petrol. Sin.* 26 (1), 165–176 (in Chinese with English abstract).
- Sun, Y.W., Li, M.S., Ge, W.C., Zhang, Y.L., Zhang, D.J., 2013. Eastward termination of the Solonker–Xar Moron River suture determined by detrital zircon U–Pb isotopic dating and Permian floristics. *J. Asian Earth Sci.* 75, 243–250. <http://dx.doi.org/10.1016/j.jseas.2013.07.018>.
- Utkin, V.P., 2013. Shear structural paragenesis and its role in continental rifting of the East Asian margin. *Russ. J. Pac. Geol.* 7 (3), 167–188. <http://dx.doi.org/10.1134/S181971401303007x>.

- Van der Voo, R., Van Hinsbergen, D.J.J., Domeier, M., Spakman, W., Torsvik, T.H., 2015. Late Jurassic–earliest Cretaceous closure of the Mongol–Okhotsk Ocean: a paleomagnetic and seismological–tomographic analysis. *Geol. Soc. Am. Spec. Pap.* 513, SPE513–SPE519.
- Wan, X.Q., Zhao, J., Scott, R.W., Wang, P.J., Feng, Z.H., Huang, Q.H., Xi, D.P., 2013. Late Cretaceous stratigraphy, Songliao Basin, NE China: SK1 cores. *Palaeogeogr. Palaeoclimatol. Palaeoecol.* 385, 31–43. <http://dx.doi.org/10.1016/j.palaeo.2012.10.024>.
- Wang, P.J., Chen, S.M., 2015. Cretaceous volcanic reservoirs and their exploration in the Songliao Basin, northeast China. *AAPG Bull.* 99 (3), 499–523. <http://dx.doi.org/10.1306/09041413095>.
- Wang, Y.J., Fan, Z.Y., 1997. Discovery of Permian radiolarians in ophiolite belt on northern side of Xar Moron River, Inner-Mongolia and its geological significance. *Acta Palaeontol. Sin.* 36 (1), 58–69 (in Chinese with English abstract).
- Wang, D.P., Liu, Z.J., Wang, P.J., Du, X.D., Liu, W.Z., Liu, L., 1991. Sedimentary Facies and Paleogeography of the Songliao Basin. Dongbei Oilfield Company Ltd., Report and Atlas of the within-Company Open File, Changchun (200 pp., in Chinese).
- Wang, P.J., Liu, W.Z., Wang, S.X., Song, W.H., 2002a. $^{40}\text{Ar}/^{39}\text{Ar}$ and K/Ar dating on the volcanic rocks in the Songliao Basin, NE China: constraints on stratigraphy and basin dynamics. *Int. J. Earth Sci.* 91 (2), 331–340. <http://dx.doi.org/10.1007/s005310100219>.
- Wang, P.J., Ren, Y.G., Shan, X.L., Sun, S.B., Wan, C.B., Bian, W.H., 2002b. The Cretaceous volcanic succession around the Songliao Basin, NE China: relationship between volcanism and sedimentation. *Geol. J.* 37 (2), 97–115. <http://dx.doi.org/10.1002/gj.905>.
- Wang, P.J., Chen, F.K., Chen, S.M., Siebel, W., Satir, M., 2006. Geochemical and Nd–Sr–Pb isotopic composition of Mesozoic volcanic rocks in the Songliao basin, NE China. *Geochem. J.* 40 (2), 149–159. <http://dx.doi.org/10.2343/geochemj.40.149>.
- Wang, P.J., Xie, X.A., Mattern, F., Ren, Y.G., Zhu, D.F., Sun, X.M., 2007a. The Cretaceous Songliao Basin: volcanogenic succession, sedimentary sequence and tectonic evolution, NE China. *Acta Geol. Sin. (Engl. Ed.)* 81 (6), 1002–1011. <http://dx.doi.org/10.1111/j.1755-6724.2007.tb01022.x>.
- Wang, P.J., Sun, X.M., Liu, W.Z., Shan, X.L., Cheng, R.H., Zheng, C.Q., 2007b. Establishment of Outcrop System and Geo-Transects of the Songliao Basin. Daqing Oilfield Company Ltd., Report and Atlas of the within-Company Open File, Daqing (312 pp., in Chinese).
- Wang, P.J., Gao, Y.F., Cheng, R.H., Wang, G.D., Wu, H.Y., Wan, X.Q., Yang, G.S., Wang, Z.X., 2009a. Description of Cretaceous sedimentary sequence of the second and third member of the Qingshankou Formation recovered by CCSD-SK-1s borehole in Songliao Basin: lithostratigraphy, sedimentary facies and cyclic stratigraphy. *Earth Sci. Front. (Online Engl. Ed.)* 16 (2), 288–313. [http://dx.doi.org/10.1016/s1872-5791\(08\)60080-9](http://dx.doi.org/10.1016/s1872-5791(08)60080-9).
- Wang, C.W., Sun, Y.W., Li, N., Zhao, G.W., Ma, X.Q., 2009. Tectonic implications of Late Paleozoic stratigraphic distribution in Northeast China and adjacent region. *Sci. China Ser. D Earth Sci.* 52 (5), 619–626. <http://dx.doi.org/10.1007/s11430-009-0062-7>.
- Wang, P.J., Gao, Y.F., Ren, Y.G., Zhang, J.G., 2009b. $^{40}\text{Ar}/^{39}\text{Ar}$ age and geochemical features of mugearite from the Qingshankou Formation: significances for basin formation, hydrocarbon generation and petroleum accumulation of the Songliao Basin in Cretaceous. *Acta Petrol. Sin.* 25 (5), 1178–1190 (in Chinese with English abstract).
- Wang, G.D., Cheng, R.H., Wang, P.J., Gao, Y.F., 2010. Coniacian seismites: structure, sequence and volcanogenic origin of Qingshankou Formation in the Cretaceous Songliao Basin. *Acta Petrol. Sin.* 26 (1), 121–129 (in Chinese with English abstract).
- Wang, J.H., Chen, H.H., Wang, H., Jiang, T., Miao, H.B., 2011. Two types of strike-slip and transtensional intrabasinal structures controlling sandbodies in Yitong Graben. *J. Earth Sci.* 22 (3), 316–325. <http://dx.doi.org/10.1007/s12583-011-0184-7>.
- Wang, T., Zheng, Y.D., Zhang, J.J., Zeng, L.S., Donskaya, T., Guo, L., Li, J.B., 2011. Pattern and kinematic polarity of late Mesozoic extension in continental NE Asia: perspectives from metamorphic core complexes. *Tectonics* 30 (6), TC6007. <http://dx.doi.org/10.1029/2011tc002896>.
- Wang, C.S., Scott, R.W., Wan, X.Q., Graham, S.A., Huang, Y.J., Wang, P.J., Wu, H.C., Dean, W.E., Zhang, L.M., 2013. Late Cretaceous climate changes recorded in Eastern Asian lacustrine deposits and North American Epicrine sea strata. *Earth-Sci. Rev.* 126, 275–299. <http://dx.doi.org/10.1016/j.earscirev.2013.08.016>.
- Wang, G.D., Cheng, R.H., Wang, P.J., Gao, Y.F., Wang, C.S., Ren, Y.G., Huang, Q.H., 2015. High resolution continuous sedimentary records of Upper Cretaceous obtained from the continental drilling (SK1) borehole in Songliao Basin: Sifangtai and Mingshui Formations. *Geosci. Front.* 6, 895–912.
- Wang, P.J., Zhao, R.L., Meng, Q.A., Qu, X.J., Zhu, D.F., Gao, Y.F., 2015. The Cretaceous Songliao Basin: dynamic background from volcanic rift to interior sag basin. *Earth Sci. Front. (Chin. Ed.)* 22 (3), 72–91. <http://dx.doi.org/10.13745/j.esf.2015.03.009> (in Chinese with English abstract).
- Wang, P.J., Chen, C.Y., Liu, H.B., 2016. Aptian giant explosive volcanic eruptions in the Songliao Basin and Northeast Asia: a possible cause for global climate change and OAE-1a. *Cretac. Res.* 62, 98–108. <http://dx.doi.org/10.1016/j.cretres.2015.09.021>.
- Wernicke, B., 1981. Low-angle normal faults in the Basin and Range Province: nappe tectonics in an extending orogen. *Nature* 291, 645–648.
- White, L.T., Lister, G.S., 2012. The collision of India with Asia. *J. Geodyn.* 56–57 (SI), 7–17. <http://dx.doi.org/10.1016/j.jog.2011.06.006>.
- Wilson, M., 1989. *Igneous Petrogenesis: A Global Tectonic Approach*. Unwin Hyman, London (466 pp.).
- Wilson, M., Lyashkevich, Z.M., 1996. Magmatism and the geodynamics of rifting of the Pripyat–Dnieper–Donets rift, East European Platform. *Tectonophysics* 268 (1), 65–81. [http://dx.doi.org/10.1016/s0040-1951\(96\)00234-x](http://dx.doi.org/10.1016/s0040-1951(96)00234-x).
- Woodcock, N.H., 1986. The role of strike-slip fault systems at plate boundaries. *Philos. Trans. R. Soc. Lond. A* 317, 13–29.
- Wu, D.Y., 1989. Magma origin of Cenozoic basalts in Yitong county, Jilin Province. *Acta Petrol. Sin.* 5 (2), 65–75 (in Chinese).
- Wu, F.Y., Lin, J.Q., Wilde, S.A., Zhang, X.O., Yang, J.H., 2005. Nature and significance of the Early Cretaceous giant igneous event in eastern China. *Earth Planet. Sci. Lett.* 233, 103–119. <http://dx.doi.org/10.1016/j.epsl.2005.02.019>.
- Wu, F.Y., Sun, D.Y., Ge, W.C., Zhang, Y.B., Grant, M.L., Wilde, S.A., Jahn, B.M., 2011. Geochronology of the Phanerozoic granitoids in northeastern China. *J. Asian Earth Sci.* 41, 1–30. <http://dx.doi.org/10.1016/j.jseaes.2010.11.014>.
- Xi, D.P., Wan, X.Q., Feng, Z.Q., Li, S., Feng, Z.H., Jia, J.Z., Jing, X., Si, W.M., 2011. Discovery of Late Cretaceous foraminifera in the Songliao Basin: evidence from SK-1 and implications for identifying seawater incursions. *Chin. Sci. Bull.* 56 (3), 253–256. <http://dx.doi.org/10.1007/s11434-010-4269-y>.
- Xu, W.L., Wang, F., Pei, F.P., Meng, E., Tang, J., Xu, M.J., Wang, W., 2013. Mesozoic tectonic regimes and regional ore-forming background in NE China: constraints from spatial and temporal variations of Mesozoic volcanic rock associations. *Acta Petrol. Sin.* 29 (2), 339–353 (in Chinese with English abstract).
- Xu, B., Zhao, P., Bao, Q.Z., Zhou, Y.H., Wang, Y.Y., Luo, Z.W., 2014. Preliminary study on the pre-Mesozoic tectonic unit division of the Xing-Meng Orogenic Belt (XMOB). *Acta Petrol. Sin.* 30 (7), 1841–1857 (in Chinese with English abstract).
- Yang, W.L., 1985. Daqing oil field, People's Republic of China: a giant field with oil of nonmarine origin. *AAPG Bull.* 69 (7), 1101–1111.
- Yang, B.J., Mu, S.M., Jin, X., Liu, C., 1996. Synthesized study on the geophysics of Mangzhouli–Suifenhe geoscience transect, China. *Acta Geophys. Sin.* 39 (6), 772–782 (in Chinese with English abstract).
- Yang, B.J., Tang, J.R., Li, Q.X., Wang, J.M., Faisal, S.A., Li, R.L., Wang, H.Z., Li, Z.L., Zhang, H., 2004. Crustal reflection structure in the uplifting of Songliao Basin and disconnecting Moho interface. *Sci. China Ser. D Earth Sci.* 47 (6), 514–521.
- Yang, J.H., O'Reilly, S., Walker, R.J., Griffin, W., Wu, F.Y., Zhang, M., Pearson, N., 2010. Diachronous decratonization of the Sino-Korean craton: geochemistry of mantle xenoliths from North Korea. *Geology* 38 (9), 799–802. <http://dx.doi.org/10.1130/g30944.1>.
- Yoon, S.H., Sohn, Y.K., Cough, S.K., 2014. Tectonic, sedimentary, and volcanic evolution of a back-arc basin in the East Sea (Sea of Japan). *Mar. Geol.* 352 (SI), 70–88. <http://dx.doi.org/10.1016/j.margeo.2014.03.004>.
- Zaigham, N.A., Mallick, K.A., 2000. Prospect of hydrocarbon associated with fossil-rift structures of the southern Indus basin, Pakistan. *AAPG Bull.* 84 (11), 1833–1848.
- Zhang, Y.X., Sun, Y.S., Zhang, X.Z., Yang, B.J., 1998. Geotraverse from Manzhouli to Suifenhe, China (Map & Guidebook). *Geol. Publ. House, Beijing* (53 pp., in Chinese).
- Zhang, X.D., Yu, J., Chen, F.J., Wang, X.W., 2000. Structural characteristics, origin and evolution of metamorphic core complex in central basement uplift and Xujiaweizi faulted depression in Songliao Basin, northeast China. *Earth Sci. Front. (Chin. Ed.)* 7 (4), 411–418 (in Chinese with English abstract).
- Zhang, Y.G., Chen, S.M., Zhang, E.H., Jiang, C.J., 2010. The new progress of Xujiaweizi fault depression characteristics of structural geology research. *Acta Petrol. Sin.* 26 (1), 142–148 (in Chinese with English abstract).
- Zheng, H., Sun, X.M., Zhu, D.F., Tian, J.X., He, S., Wang, Y.D., Zhang, X.Q., 2015. The structural characteristics, age of origin, and tectonic attribute of the Erguna fault, NE China. *Sci. China Earth Sci.* 58 (9), 1553–1565. <http://dx.doi.org/10.1007/s11430-015-5144-0>.
- Zhou, J.B., Wilde, S.A., Zhao, G.C., Zhang, X.Z., Zheng, C.Q., Wang, H., 2010a. New shrimp U–Pb Zircon ages from the Heilongjiang high-pressure belt: constraints on the Mesozoic evolution of NE China. *Am. J. Sci.* 310 (9), 1024–1053. <http://dx.doi.org/10.2475/09.2010.10>.
- Zhou, J.B., Wilde, S.A., Zhao, G.C., Zhang, X.Z., Zheng, C.Q., Wang, H., Zeng, W.S., 2010b. Pan-African metamorphic and magmatic rocks of the Khanka Massif, NE China: further evidence regarding their affinity. *Geol. Mag.* 147 (5), 737–749. <http://dx.doi.org/10.1017/s0016756810000063>.
- Ziegler, P.A., 1982. *Geological Atlas of Western and Central Europe*. Shell, Amsterdam (130 pp.).
- Zorin, Y.A., 1999. Geodynamics of the western part of the Mongolia–Okhotsk collisional belt, Trans-Baikal region (Russia) and Mongolia. *Tectonophysics* 306 (1), 33–56. [http://dx.doi.org/10.1016/s0040-1951\(99\)00042-6](http://dx.doi.org/10.1016/s0040-1951(99)00042-6).
- Zyabrev, S.V., 2011. Stratigraphy and structure of the central East Sakhalin accretionary wedge (Eastern Russia). *Russ. J. Pac. Geol.* 5 (4), 313–335. <http://dx.doi.org/10.1134/s1819714011040087>.